2017•2018
Faculteit Industriële ingenieurswetenschappen
master in de industriële wetenschappen: bouwkunde

Masterthesis
Modelling of the anchorage zone of prestressed concrete elements

PROMOTOR :
ing. Rik STEENSELS

COPROMOTOR :
Prof. dr. ing. Bram VANDOREN

Alexander Schraeyen, Lennert Vanbuel

Scriptie ingediend tot het behalen van de graad van master in de industriële wetenschappen: bouwkunde

De transnationale Universiteit Limburg is een uniek samenwerkingsverband van twee universiteiten in twee landen: de Universiteit Hasselt en Maastricht University.

Universiteit Hasselt | Campus Diepenbeek | Agoralaan Gebouw D | BE-3590 Diepenbeek
Universiteit Hasselt | Campus Hasselt | Martelarenlaan 42 | BE-3500 Hasselt

2017 • 2018

Faculteit Industriële ingenieurswetenschappen

master in de industriële wetenschappen: bouwkunde

Masterthesis

Modelling of the anchorage zone of prestressed concrete elements

PROMOTOR :
ing. Rik STEENSELS

COPROMOTOR :
Prof. dr. ing. Bram VANDOREN

Alexander Schraeyen, Lennert Vanbuel

Scriptie ingediend tot het behalen van de graad van master in de industriële wetenschappen: bouwkunde

UHASSELT KU LEUVEN

Preface

This master's thesis was conducted in the context of the master's degree in Civil Engineering Technology at Hasselt University in association with Catholic University of Leuven. Construction Engineering Research Group, abbreviated as CERG is a part of the research group at Hasselt University which includes this research. CERG mainly investigates the behaviour of brittle and quasi-brittle structural components like concrete and masonry using a finite element model [1]. The acquired knowledge will be converted into a matter that is usable for the industry. This research belongs to this research domain of the research group.

The elaboration of this study was not possible without the help of a certain person. We would like to thank ing. Rik Steensels who contributed to an efficient progress of this master's thesis. He gave us the knowledge for this research with reference to his doctoral research. He was always available to give explanations and to guide us during this research.

Finally, we would like to thank our friends and family for the help and the opportunity to obtain the master's degree in Civil Engineering Technology.

Table of content

List of tables

List of figures

Glossary

Term	Declaration
FEA	Finite Element Analysis
FEM	Finite Element Method
I700UL	I700 beam with upper and lower reinforcement
R400L	R400 beam with only lower reinforcement
R400UL	R400 beam with upper and lower reinforcement
STM	Strut-and-tie model
Struts	The struts will represent the concrete and will distribute the compressive stresses
Ties	The ties will represent the reinforcement and will distribute the tensile stresses

Abstract

I-shaped prestressed concrete beams are commonly used as bridge girders. Due to the prestressing of the horizontal strands, the prestress force needs to be transferred to the concrete. As a result of this stress distribution, vertical tensile stresses are induced in the anchorage zone which may lead to horizontal cracks. In order to counteract this cracking, vertical reinforcement is placed in this specific zone. This research includes optimising the vertical reinforcement and minimizing the cracking pattern. Moreover, safety factors are implemented to make the model practically usable.

First, non-linear three dimensional numerical models are used to determine the flow of forces in the anchorage zone. Afterwards, strut-and-tie models can be set up, based on the flow of forces on vector plots generated by the numerical model. Based on the strut-and-tie model, the necessary reinforcement can be calculated. Thereafter, safety factors are implemented to achieve a realistic and safe amount of reinforcement.

A correlation has been found to adapt the lever arm depending on the percentage of prestress loss to maintain the same reinforcement as before the prestress loss. This adjustment acts as a safety factor. This safety factor which takes into account the prestress losses will probably not suffice, an additional safety factor of 1,3 is recommended to be multiplied by the prestress force. Finally, an attempt is made to optimise the strut-and-tie model provided by R. Steensels, but a fully optimised model is not found.

Abstract in het Nederlands

Voorgespannen balken met een I-vormige doorsnede worden gebruikt als brugliggers. Het voorspannen van de horizontale wapening zorgt ervoor dat de voorspankracht moet worden overgebracht naar het beton. Deze spanningsverdeling induceert verticale trekspanningen in de verankeringszone met mogelijke scheurvorming als gevolg. Om dit te vermijden wordt in deze zone verticale wapening geplaatst. Dit onderzoek bevat de optimalisatie van de verticale wapening en de minimalisatie van de scheurvorming. Bovendien worden veiligheidsfactoren geïmplementeerd om het model praktisch toepasbaar te maken.

Eerst werd een niet-lineair, driedimensionaal numeriek model gebruikt om de krachtswerking in de verankeringszone te bepalen. Vervolgens werd een *strut-and-tie model* opgesteld dat gebaseerd is op spanningstrajectoren. Aan de hand van dit model kan de nodige hoeveelheid wapening berekend worden. Hierna worden veiligheidsfactoren geïmplementeerd om een realistische en veilige hoeveelheid wapening te verkrijgen.

Er werd een correlatie gevonden om de hefboomsarm aan te passen aan de hand van de voorspanningsverliezen. Dit werd gedaan om dezelfde wapening te houden als voor de voorspanningsverliezen in rekening werden gebracht. Deze aanpassing doet dienst als veiligheidsfactor, maar zal waarschijnlijk niet voldoende zijn. Daarom wordt een extra veiligheidsfactor van 1,3 op de voorspankracht aanbevolen. Tot slot werd een poging gedaan om het *strut-and-tie model* te optimaliseren, maar een volledig optimaal model werd niet gevonden.

1 Introduction

1.1 Situating

Prestressed concrete is becoming more common in civil engineering technology. Floor slabs and structural components like columns and beams are often used as structural components in buildings. Another application is to use prestressed concrete beams as bridge girders or roof girders [2]. These girders are mostly I-shaped with prestressed strands in the lower flange and optionally also in the upper flange. The cross-section of the beam has the shape of the letter I to achieve a higher moment of inertia in comparison with a rectangular beam with the same amount of concrete. The greater the moment of inertia, the greater the resistance to bending. The beams have a complex structure due to the shape of the cross-section and the prestressed strands. Hereby, the beams are fabricated at precast plants. These prefabricated beams have the advantage to reach a high level of quality and a reduction of working costs due to the optimised construction times on the construction site because no pouring of the concrete is necessary [3]. Due to horizontal prestressing strands, it is possible to achieve longer spans or a higher bearing capacity by using the materials more efficiently.

Since the value of the prestress load became significantly larger through the years, also the tensile stresses in the end zone of the beam became larger. A good knowledge of these distribution of stresses is important to counter some of the problems occurring due to this increase of prestressing [4]. The anchorage zone, also named as the end zone, is a critical place which needs further investigation. At this place, the prestress force is transferred from the prestress strands to the concrete. Due to this stress distribution, the anchorage zone is subjected to vertical tensile forces which leads to horizontal cracks. In order to counteract this cracking, vertical reinforcement is placed in this specific zone. Due to a lack of knowledge and techniques to efficiently calculate this reinforcement, a larger amount of reinforcement is placed than necessary for safety reasons.

1.2 Objectives

In the current society, it is important to increase the efficiency of the use of building materials in a durable and sustainable way. The increased efficiency of the use of materials leads to a more efficient economic result of the construction, especially the construction components. In addition, this economic improvement is nowadays necessary in an oligopolistic industry[1]. The cracking behaviour will negatively affect the durability of the element. It is important to minimize or preferably avoid large cracks. At the moment, the vertical reinforcement is calculated by using a numerical model with some simplifications. As stated before, this model is not optimised which leads to an overestimation of the vertical reinforcement. Moreover, some performed beams show still a non-negligible cracking pattern in the anchorage zone. This research determines the theoretical background of the anchorage zone, making it possible to perform an optimisation of the vertical reinforcement and minimize the cracking pattern.

Next, safety factors need to be implemented to achieve a model that is practically applicable. Finally, the problem is considered solved if a model is achieved in which the crack formation is limited and the calculated amount of reinforcement has a realistic and minimal value.

[1] An oligopolistic industry is a market in which a product is offered by only a few large suppliers [26].

1.3 Method

It is necessary to have a good understanding of the interaction between the concrete and the prestressing strands, and the flow of forces induced by transferring the prestress from the tendons to the concrete. Therefore, this research was started with conducting a literature review. Thereafter, three dimensional numerical models are used to determine the flow of forces in the anchorage zone. The non-linear softening behaviour of concrete and the loss of confinement due to the occurrence of cracks were taken into account. After achieving the necessary knowledge, strut-and-tie models can be set up based on the numerical models. Based on these strut-and-tie models the necessary reinforcement can be calculated. By performing a geometric optimisation of the strut-and-tie model a realistic and minimal value of vertical reinforcement can be achieved.

Next, this research contains the translation from theory to practice by implementing safety factors in the numerical model. This is done by applying the European safety regulations to the final and most optimal model. Material properties and prestress losses are taken into account to achieve an actually and safe result.

1.4 Synopsis

A short overview of each chapter is given to get a better understanding of the complete research. Chapter 2 states some general principles and definitions to explain the different phenomena occurring during the prestressing of a beam. These different phenomena named bursting, spalling and splitting are first clarified. In the last part of this chapter the cracks of bursting, spalling and splitting are displayed and explained how these cracks will propagate in practice.

Chapter 3 explains the different concepts used to design a strut-and-tie model (STM) and an example is given of how a strut-and-tie model is elaborated. The first part of this chapter outlines the fundamentals of a STM and where and when this kind of model is used. In a second part of this chapter the calculations of the struts, ties and nodes advised by Eurocode 2 and Model Code 2010 are displayed. In the last two sections of this chapter a procedure of how to make a STM, developed by C. Williams will be explained. Additionally, this procedure of C. Williams will be elaborated to demonstrate how the STM used in this research could have been developed.

In chapter 4 the different models that already were developed in the past are summarized. The first model developed is the model of Marshall & Mattock who experimentally determined an equation to calculate the required area of end zone reinforcement. A second model is the AASHTO regulation that originates from America who require that a four percent of the prestressing force is used as the tensile force. For this tensile force must be placed vertical reinforcement at the end zone of the girder. This is a conservative version of Marshall & Mattock's model. Next, Gergely & Sozen made an analysis which is based on the equilibrium of the cracked section and can determine the spalling force and also predict where the first crack is going to appear. In the last paragraph Davis & Crispino conducted a numerical model and is calibrated with a case study.

Chapter 5 is a literature study to better understand the modelling approach of the bond-slip behaviour between the steel and concrete. Also the transfer length of the prestressing strands to the concrete is studied. A two-staged modelling approach is conducted. The first stage is describing the bond-slip behaviour and the transfer length. Next, in the second stage this behaviour is used to finite element model to calculate the anchorage zone stress field.

In the next chapter, chapter 6, the safety factors and prestress losses are discussed. This chapter can be divided in three general parts. In this first part the need for safety factors in the design of constructional elements is explained. The second part of this chapter summarises all different kinds of prestress losses and will indicate which losses are relevant to take into account to this research. One general reduction factor for the prestress force is given in favourable conditions and a safety factor for prestress forces in unfavourable conditions is given. In the last part of this chapter these safety factors for the prestressing losses are implemented and further examined.

An attempt to optimise the strut-and-tie model developed by R. Steensels is made in chapter 7. In the first part the different beams used in this research are shown. The geometrical properties of the beams and the used amount of reinforcement is displayed. In a second part a first attempt is made to optimise the strut-and-tie model by varying the lever arm of the model. When varying the lever arm, different deformations will arise, these deformations can be transformed into energy. When comparing these amounts of energy, the most efficient model can be determined. In the last part of this chapter the all-over geometry of the struts and ties of the model are adapted to find a more efficient model.

2 Cracks caused by tensile forces

Since the value of the prestress load became significantly larger through the years, also the tensile stresses in the end zone of the beam became larger. A good knowledge of these distribution of stresses is important to counter some of the problems occurring due to this increase of prestressing [4]. The anchorage zone, also named as end zone, is the part of the beam starting at the end of the girder and ending at the transmission length. To define this transmission length, it is required to explain some other terminology. The transfer length is defined as the length which is needed to transfer the prestress force of the tendon to the concrete. The transfer of the prestressing force to the tendons and the concrete depends on the bond behaviour. The bond behaviour depends on the adhesion between steel and concrete. The better the adhesion, the shorter the transfer length will be. After releasing the jack or flame cutting when the prestressing force is applied, the force needs to be transferred to the element. In the end zone of the beam there will be no prestress force because the tendons will pull back after cutting those. So as mentioned before, the transfer length will depend on the bond behaviour. The shorter the transfer length, the bigger the tensile stresses in the vertical axis because the pretensioning force will remain the same but will act on a smaller surface. The axial stress in the tendons will disperse until a constant axial stress is achieved, named prestress value. This prestress value often has a value of 80% of the yield strength of the steel, this prestress value will be smaller for the concrete because there is a larger surface of concrete to distribute these forces. The length beginning from the end of the beam and ending at the point where a linear distribution of stresses is reached in the steel tendons, is called transmission length.

The stress behaviour in the anchorage zone needs to be considered further to avoid cracks which could lead to structural damage or failure. It is also important to avoid cracks for aesthetic and durability reasons [5].

2.1 Bursting

There are three types of tensile stresses in the anchorage zone which could lead to cracking. The first stress behaviour, bursting stress, occurs at a small distance from the end as can be seen in Figure 1. By transferring the prestress force, high compressive stresses arise on the concrete. These compressive forces are distributed over the concrete surface in a curved pattern. Due to this curved propagation over the length, tensile forces in different directions will arise. The vertical component of these resulting stresses is a normal stress, acting perpendicular to the axis of the prestressed tendon [6]. Due to these vertical tensile forces withdrawal of the concrete from the tendon occurs.

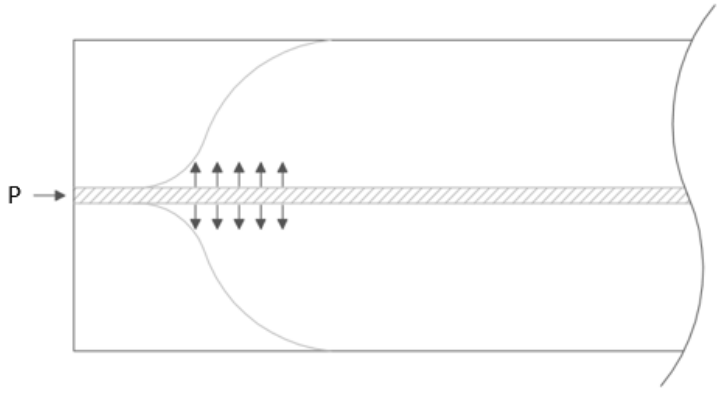

Figure 1 - Bursting

Model code 2010 [5] suggests the following calculation based on a prismatic component, depicted in Figure 2. The length of the prism can be calculated with equation 2.1:

$$l_{bs} = \sqrt{h_{bs}^2 + (0{,}6L_{bpt})^2} < l_{bpt} \tag{2.1}$$

Where L_{bpt} is the transmission length and h_{bs} is the height of the prism. The internal lever arm for the bursting force is:

$$Z_{bs} = 0{,}5 l_{bs}$$

The bursting force N_{bs} can be determined by writing down the moment equilibrium along section A-A of the prism seen in Figure 2:

$$N_{bs} = \frac{\frac{1}{2}(n_1+n_2)t_2 - n_1 t_1}{Z_{bs}} \gamma_1 F_{sd} \tag{2.2}$$

Where:

t_1 is the distance between the centroid of the prestressing strands above the section to the centroid of the prism

t_2 is the distance between the centroid of the concrete stress block above the section to the centroid of the prism

n_1, n_2 are respectively the amount of tendons above and below the section

F_{sd} the design prestress force for each tendon

$\gamma_1 = 1.1$ the safety factor used to take into account overstressing

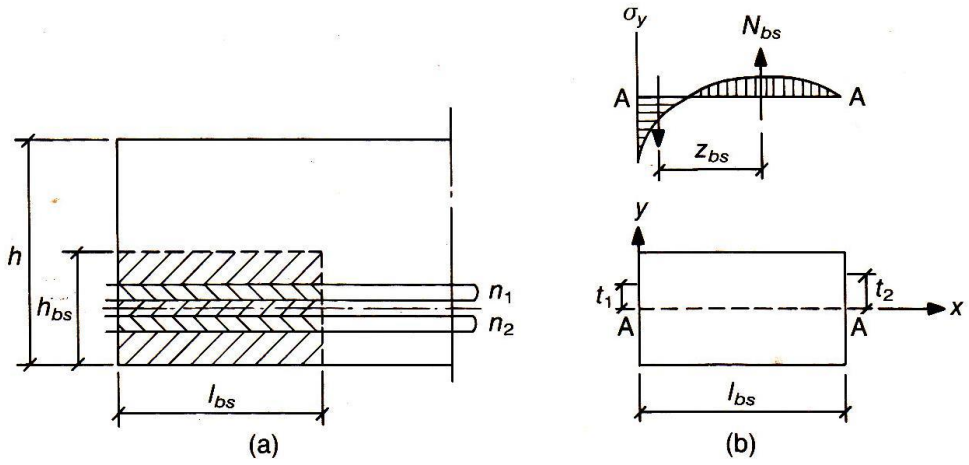

Figure 2 - (a) Dimensions of the symmetrical prism; (n) moment equilibrium along section A-A [5, p. 234]

The maximum bursting stress:

$$\sigma_{bs} = \frac{N_{bs}}{b_{bs} \,.\, l_{bs}} \tag{2.3}$$

If $\sigma_{bs} < f_{ctd}$, no bursting reinforcement is required!

2.2 Spalling

The second stress behaviour is spalling, which would be visual in case of eccentric reinforcement. Spalling will also happen in case of centric reinforcement, but it will not be visible in practice. Due to the axial tensile forces of the tendons, compressive stresses arise in some zones of the concrete. As an example in Figure 3, the hatched zone will be subject to compressive stresses. The compressed area is influenced by the eccentricity of the tendon and the cross-section of the girder. The concrete close to the tendons will displace along with the tendons as a result of the bond behaviour. The concrete in the top of the beam will not be affected by the tendon. This causes a different deformation in the section of the concrete, represented by the blue line. This would lead to tensile stresses, called spalling, due to ensure the compatibility of displacements.

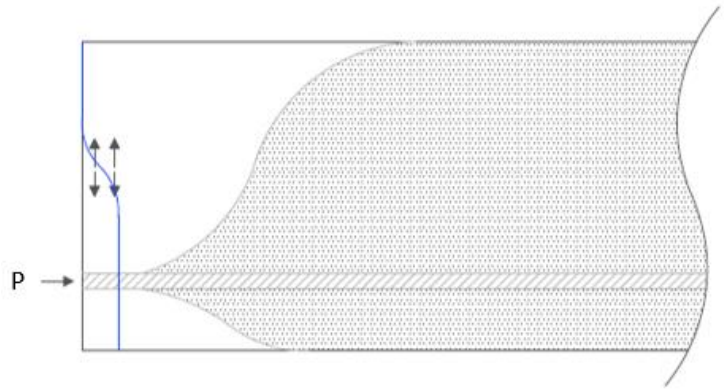

Figure 3 - Spalling

The spalling forces can be determined by using Figure 4, which is based on elastic analysis. This graph is only valid for members with a maximum height of 400mm. No other method for bigger elements is provided by the Model Code. The maximum spalling stress is in function of the eccentricity of the tendons and the transmission length.

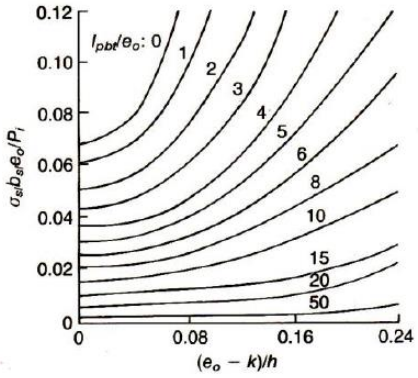

Figure 4 - Maximum spalling stress [5, p. 235]

2.3 Splitting

The last stress behaviour is named splitting stresses. These stresses are a result of the 'Poisson effect'. When the prestress load is put on the reinforcement, the tendon's cross-section will decrease due to the Poisson effect as can be seen in Figure 5. After releasing the jack or flame cutting the tendon, its cross-section will increase again to the original dimensions. In this state of the process, the concrete already hardened and will counteract the widening of the tendons. The axial forces in the tendons leads to circumferential stresses which could lead to radial cracks.

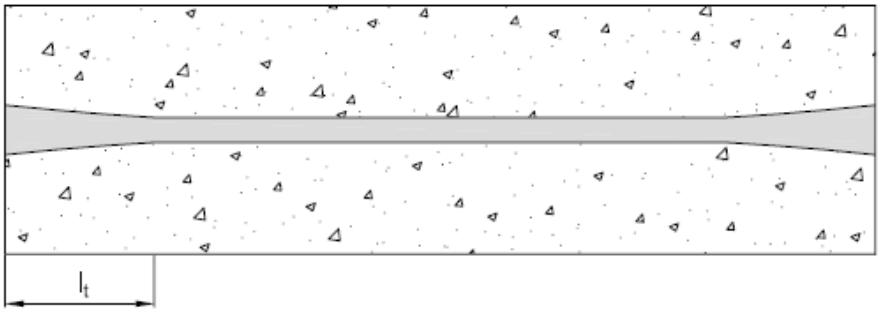

Figure 5 - Splitting stresses from Poisson effect [4, p. 9]

Model code 2010 advices to place no reinforcement for the acting splitting forces, but only if the distance from the strands to the concrete cover meet the minimum values given in Table 1. The concrete cover depends on the strength of the concrete and spacing between the tendons.

Table 1 – Minimum concrete cover [2, p. 236]

Concrete strength	Clear spacing	Cover
C20/25 to C50/60	≥ 3ϕ < 3ϕ	≥ 3ϕ ≥ 4ϕ
≥ C55/67	≥ 2ϕ	≥ 2ϕ

2.4 The three different cracking patterns in practice

Figure 6 shows a beam with cracks on the end of the beam. The diagonal crack, indicated with letter a, is a result of the production process. When the beam is lifted up when the concrete is hardened, the beam will bend due to the self-weight. Diagonal cracks will arise due to this deformation of the beam. This cracking can initially simply be limited by strategically placing the lifting provisions [6]. The diagonal crack can also be a result of the draped strands which sometimes are used in American prestressed beams. Draped strands are prestressed stands from the top end of the beam through the lower part in the middle of the beam. These strands can be used to enhance the capacity of the beam [7].

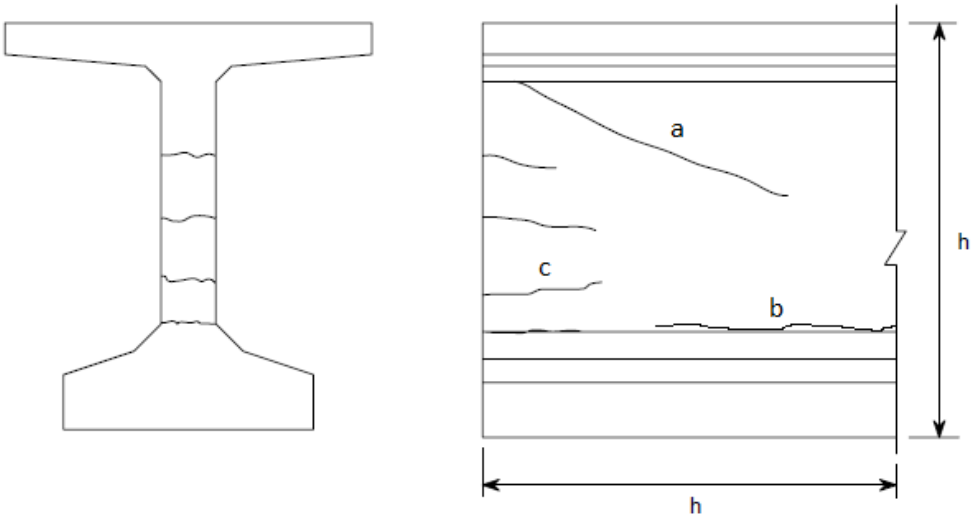

Figure 6 - Crack patterns [6, p. 3]

The other cracks in Figure 6 are derived from the three types of stresses. Bursting stresses, indicated with letter b, leads to horizontal cracks at the height of the prestressed tendons. As mentioned before, these cracks will be visible at a short distance from the end of the girder. Spalling cracks are visible at the end of the beam due to vertical tensile stresses which are a consequence of the deformation in the section of the concrete. Spalling cracks take place at a height of one third of the beam in case of a beam with only lower reinforcement. If both lower and upper reinforcement is present, spalling cracks can take place over the entire height of the beam, this is depicted in Figure 7. Spalling cracks are indicated with letter c in Figure 6. Finally, splitting stresses causes splitting cracks which probably are not visible at the outside of the beam thanks to the presence of the concrete cover. Figure 8 shows the appearance of the splitting cracks.

Figure 7 - Spalling cracks [6, p. 32]

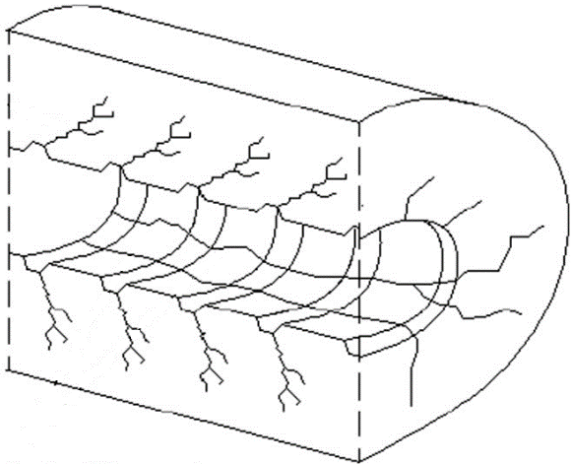

Figure 8 - Splitting cracks [8, p. 102]

3 Strut-and-tie model

A strut-and-tie model (STM) is often used to design special geometries in concrete constructions. This chapter explains the different concepts used to design a strut-and-tie model. In section 3.1 a brief introduction is made to explain why these models are used and where they should be used. In section 3.2 and section 3.3 the calculation of the struts, ties and nodes in respectively the Eurocode and the Model Code are shown. Section 3.4 is about the development of a STM, a nine step procedure by C. Williams is explained in general. This nine step procedure has been elaborated in section 3.5 for the beams used in this research to explain how the strut-and-tie model of the research of R. Steensels has been attained by using the method of C. Williams. The last section, section 3.5, describes how R. Steensels obtained his strut-and-tie model which is used to be further optimized.

3.1 Fundamentals of a strut-and-tie model

3.1.1 D-regions & B-regions

D-regions are disturbed regions or discontinuities that arise in the proximity of a load or geometrical discontinuities. An applied load, support reactions, openings, frame corners are all examples of discontinuities. It is assumed that D-regions extend a distance d from the applied load or support reactions. Where d is defined as the distance between the upper fibre of the concrete and the centre of the primary reinforcement [9]. This is only true for a point-load or support reactions, in other cases the distance d will be function of the transmission length. Figure 9 illustrates these concepts.

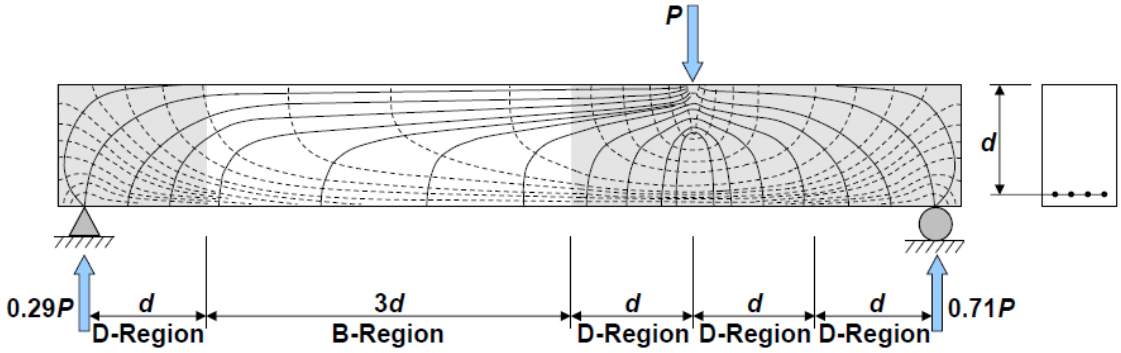

Figure 9 - Illustration of the difference between D-regions and B-regions [9, p. 5]

The B in B-regions stands for Bernoulli. The cross-sections in B-regions will remain plane in agreement with the primary beam theory, suggesting that a linear distribution of stresses occurs over the depth of the member. Therefore, the design procedure is on a section-by-section basis. B-regions will occur in between the disturbed regions.

Where non-standard elements or parts from elements of concrete structures cannot be calculated by normal beam theory, a strut-and-tie model is used. These regions cannot be calculated by normal beam theory because there are complex variations of strain occurring close to sudden changes in geometry or concentrated forces [10]. For example when calculating; piles, caps, corbels, deep beams, beams with holes, connections, etc. It is a simple method which is based on truss analogy which expresses stress patterns as a finite element model or a strut-and-tie model. In brief, it is a very powerful engineering tool where the engineer can stay in control. STM is known as a lower bound plastic theory which means it is a safe approach, because [11]:

- the design has enough ductility for the struts and ties to develop;
- the struts, ties and nodes can resist the design forces;
- equilibrium is met.

There is no single solution, each model that meets the definitions provided above will result in a realistic amount of reinforcement. Contrarily, the efficiency of each strut-and-tie model will vary. When the geometry is changed, the amount of reinforcement will change too. An optimal design can be found, where the least amount of reinforcement will be used to resist the acting forces.

3.1.2 Fundamentals

A simple strut-and-tie model is depicted in Figure 10 , describing the rough flow of forces through a simply supported beam. The ties will represent the reinforcement, which will distribute the tensile stresses. The struts will represent the concrete, these will distribute the compressive stresses. These two will intersect at nodes. The nodes are the most stressed parts in a STM, due to the concentration of stresses when two or more trusses intersecting in this node. When developing a certain model, the struts and ties need to be placed upon the flow of forces indicated by a finite element model, an elastic analysis. This will ensure a safe design with minimal cracking according to C. Williams [9].

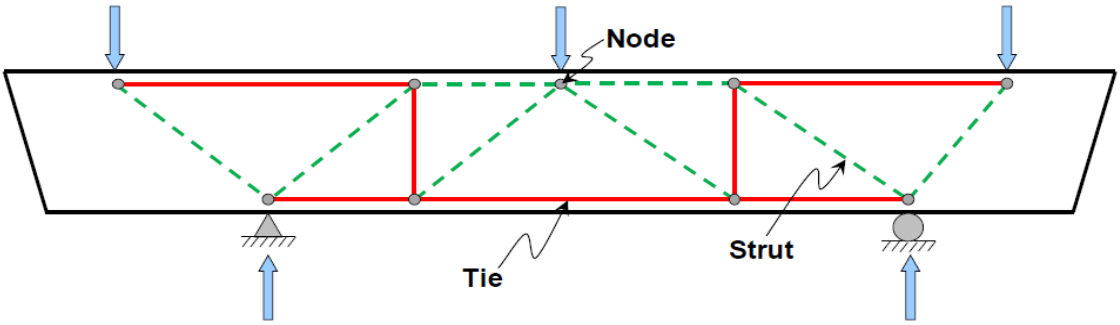

Figure 10 - The struts, ties and nodes of a STM [9, p. 7]

3.2 Eurocode 2: strut-and-tie model

Eurocode does not mention how a strut-and-tie model works or is designed, it only describes how to calculate the different stresses within the nodes, struts and ties. Specific attention should be given to the following aspects of the calculation of a STM design and only where a non-linear strain distribution exists, STM may be used. All formulas used in this paragraph originate from Eurocode 2 [12].

3.2.1 Struts

A difference has been made between the struts without transverse stresses and with transverse stresses. In a region without transverse stresses, the design strength of the strut is the same as the design compressive concrete strength as expressed in equation 3.1.

$$\sigma_{Rd,max} = f_{cd} \tag{3.1}$$

In a region with transverse stresses, the design strength for a strut may be computed from the following expression with f_{ck} the characteristic compressive strength of concrete:

$$\sigma_{Rd,max} = 0{,}6.\nu.f_{cd} \tag{3.2}$$

$$\nu = 1 - \frac{f_{ck}}{250} \tag{3.3}$$

3.2.2 Ties

The design strength of transverse ties and reinforcement should be limited. Also the reinforcement should be sufficiently anchored in the nodes. The tensile force can be calculated by:

a) Partial discontinuity regions (B- and D-regions) (b ≤ H/2)

$$T = \frac{1.(b-a)}{4.b} F \tag{3.4}$$

With a the diameter of the tie and b the effective width of a tie which can be calculated using the following equation, this width is indicated in Figure 11:

$$b_{eff,x} = d_{s01x} = \min\left(0{,}5\,.\,d_s + 0{,}65\,.\,min\left(\frac{a_0}{2.sin(\theta)}; \frac{d_s}{2}\right);\ 0{,}6\,.\frac{d_s}{tan(\theta)}\right) \tag{3.5}$$

$$b_{eff,y} = d_{s01y} = \min\left(0{,}5\,.\,d_s + 0{,}65\,.\,min\left(b_0; \frac{d_s}{2}\right);\ 0{,}6\,.\frac{d_s}{tan(\theta)}\ ; B\right) \tag{3.6}$$

Where d_s is the total length of the tie, θ is the angle between the connection of the tie and the tie itself. a_0 and b_0 is respectively the height of the element and the width of the element where an influence of the acting force can be found. B is the depth of the element, the spreading of the forces cannot be bigger than the element itself. F is the internal force in the tie that results from the prestressing force, this force can be obtained by using the geometrical formulas.

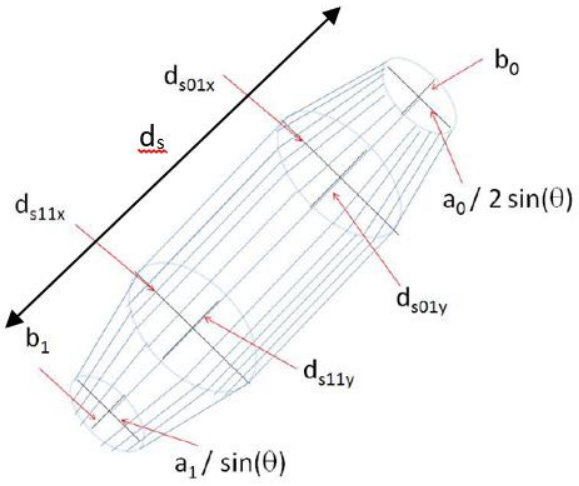

Figure 11 - Dimensions of a tie

b) Full discontinuity regions (D-regions) (b > H/2)

$$T = 0{,}25\,.\left(1 - 0{,}7\frac{a}{h}\right).F \tag{3.7}$$

With F the internal force in the tie that results from the prestressing force, this force can be obtained by using the geometrical formulas. The geometric properties a, b and h are shown in Figure 12 and can be calculated in the same way as equation 3.6 and equation 3.8.

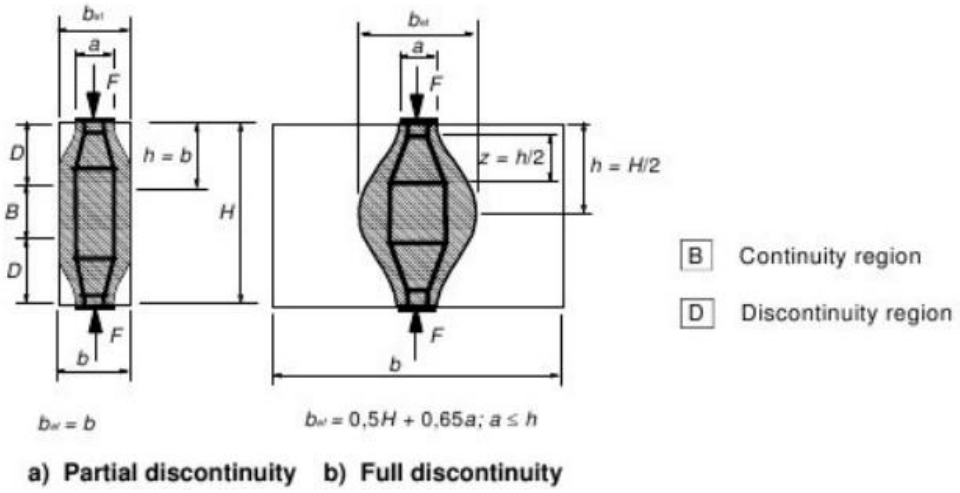

Figure 12 – Geometric properties of the ties to determine the tensile forces [12, p. 108]

3.2.3 Nodes

Several rules are applied to the nodes of a strut-and-tie model. These rules can be found in Eurocode 2 section 6.5.4 [12]. The design compressive stresses of the nodes are depending on the situation and may be calculated by:

a) In compression nodes where no ties are anchored at the node is depicted in Figure 13.

$$\sigma_{Rd,max} = k_1 \nu f_{cd} \tag{3.8}$$

k_1 = 1,0 (safe assumption, recommended value)

ν is calculated according to equation 3.3

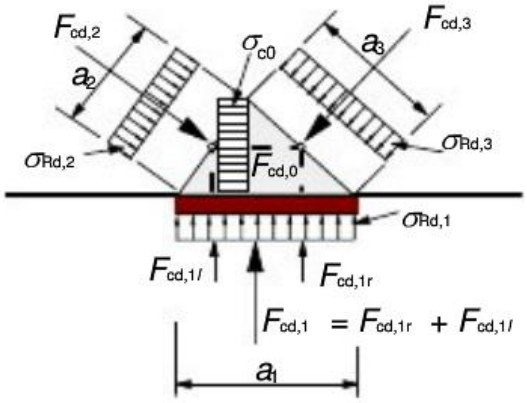

Figure 13 - Compression node without ties [12, p. 109]

b) In compression – tension nodes with anchored ties provided in one direction is depicted in Figure 14.

$$\sigma_{Rd,max} = k_2 \nu f_{cd} \tag{3.9}$$

k_2 = 0,85 (safe assumption, recommended value)

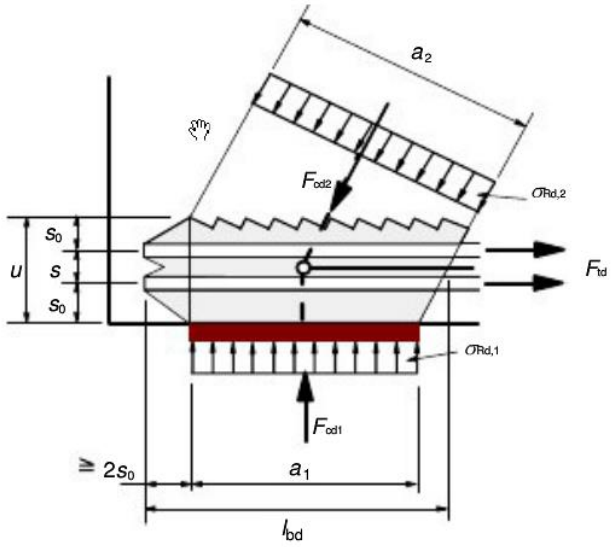

Figure 14 - Compression tension node with reinforcement provided in one direction [12, p. 109]

c) In compression – tension nodes with anchored ties provided in more than one direction is depicted in Figure 15.

$$\sigma_{Rd,max} = k_3 \nu f_{cd} \tag{3.10}$$

k_3 = 0,75 (safe assumption, recommended value)

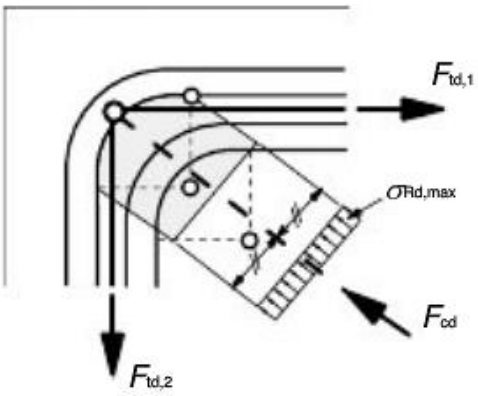

Figure 15 - Compression tension node with reinforcement provided in two directions [12, p. 110]

3.3 Model code 2010: strut-and-tie model

The Model code 2010 (MC2010) describes a strut-and-tie model but still vague [5]. The calculations for the design values for the different elements are given with almost the same approach as Eurocode 2.

3.3.1 Struts

In general the design compressive strength is calculated as follows:

$$\sigma_{Rd,max} = \frac{k_c f_{cd}}{\gamma_c} \tag{3.11}$$

f_{cd} = compressive strength concrete

γ_c = safety factor concrete = 1,5

The reduction factor k_c is as follows:

$$k_c = 0{,}75\left(\frac{30}{f_{ck}}\right)^{1/3} \leq 0{,}8 \tag{3.12}$$

This equation is only valid if there is tension normal to the direction of compression. Other cases are also mentioned in MC2010 but are less relevant to this research.

3.3.2 Ties

The strength of ties may be assumed as:

$f_{yd} = \frac{f_{yk}}{\gamma_s}$ for normal strength steel

f_{yk} = yield strength steel

γ_s = safety factor steel = 1,15

$f_{pd} = \frac{f_{p0.1k}}{\gamma_s}$ for prestressing steel

$f_{p0.1k}$ =the characteristic 0,1% proof stress

γ_s = safety factor steel = 1,15

3.3.3 Nodes

To calculate the design compressive strength of the nodes, equation 3.11 is used.

3.4 Strut-and-tie modelling by C. Williams

C. Williams described the STM procedure in nine steps depicted in Figure 16 [9]:

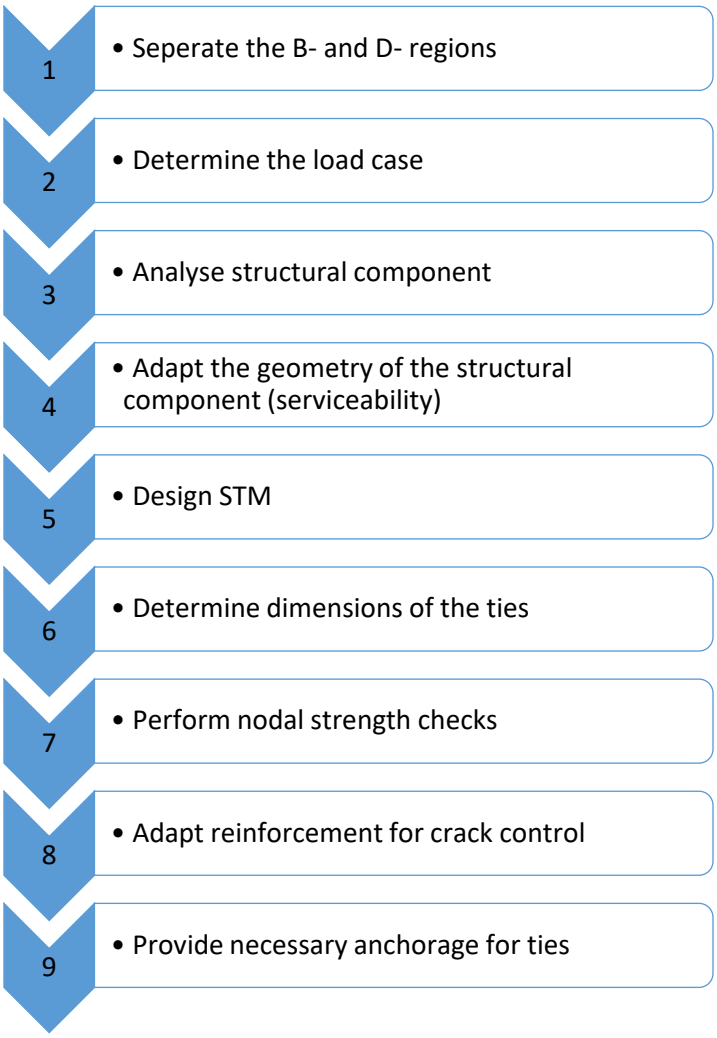

Figure 16 - Procedure of a STM [9, p. 10]

Each step of the flowchart is elaborately explained in section 3.5. All steps of the flowchart are explained briefly beneath [9]:

1. Separate B- and D-regions – Determine which parts of the beam are going to encounter normal beam theory or should the entire beam be designed using a STM.
2. Determine the load case – Compute the different design loads for each load case which act on the beam. When required, make some simplifying assumptions to develop a load case which can be applied to a strut-and-tie model.
3. Analyse structural component – Determine the reaction forces on the basis of a linear elastic analysis.
4. Adapt the geometry of the structural component (serviceability) – First the critical shear force for serviceability is checked, if the effective load is higher, it is likely diagonal cracks will form. The designer may choose to accept these risks (durability risks, aesthetic) or he can change the geometry of the member.

5. Design STM – Position the trusses to follow the actual flow of forces within the beam and calculate the forces in all trusses.
6. Determine dimensions of the ties – Calculate the reinforcement necessary to bear the acting stresses in each tie.
7. Perform nodal strength checks – Define the geometry of the critical nodes and make sure the strength of each face is sufficient to resist the applied forces calculated in the analysis of the STM.
8. Adapt reinforcement for crack control – Specify the required reinforcement for crack control to prevent diagonal cracks from occurring due to the transverse tensile stresses.
9. Provide necessary anchorage for ties – Make sure that the reinforcement is anchored accurately in the nodal regions.

3.5 Example strut-and-tie model procedure by C. Williams

To clarify this method given by Mr. Williams [9] in paragraph 2.1 an example is provided below which is applied to this research. The result of this strut-and-tie model is the model that is used in the research of R. Steensels [4]. The nine steps of this procedure are depicted in Figure 16. An R400 beam is used with a height and width of 400mm. Each step is explained independently in the different sections, however the designer will sometimes perform some steps simultaneously.

3.5.1 Step 1: Separate B- and D-regions

In the first step the beam is divided into B- and D-regions. In this model, only the part where a D-region exists is considered. The length of the D-region is exactly the same length as the transmission length of the beam, as depicted with distance d in Figure 17. The transmission length is the length where a non-linear distribution of stresses occurs, based on St. Venant's principle. Once passed this transmission length, sectional behaviour is dominating and sectional design approach can be used again. For this research it is unimportant what happens in the B-region of the beam because the cracks will only occur on the end of the beam. Hence, only the D-region is considered and will be used to design the strut-and-tie model. In Figure 17, the part that is considered is framed in red, thus only consisting of D-regions. Because there are supports on both sides of the beam, both sides may be used but they are symmetrical. In this example the left side of the beam will be used.

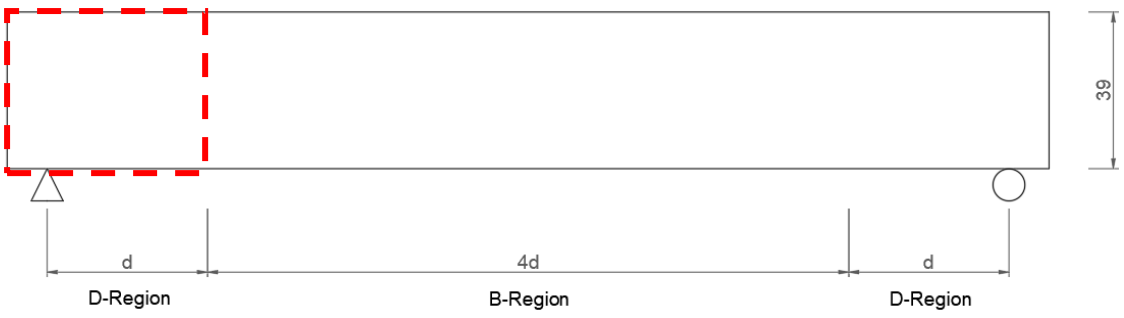

Figure 17 - Step 1: Separate B- and D-regions

3.5.2 Step 2: Determine the load case

In this next step of the design procedure, the loads that will be applied to the beam are examined. For each different critical load case, a different analysis should be performed. Since there is only one load case, only one geometry of the STM must be designed. The loads applied, that are used in this research, are only the acting forces of the prestressing strands and the reaction forces of the prestressing

strands. Due to the eccentricity of the tendons in case of a beam with only lower strands, the resulting moment needs to be equilibrated by a tensile force T and a compressive force C. For elements with both upper and lower prestressed tendons, it is no longer necessary to determine the forces T and C. This principle is further explained in section 3.6.2. Self-weight on this beam is neglected.

It is important to know that a moment cannot be applied to a STM, the moment should be separated into a couple of acting forces to achieve an equivalent moment. Point loads at a very proximity to each other may be added, the decision to do this or not is up to the designer. A distributed load has to be divided into a number of point loads that will recreate the distributed load or self-weight. These load forces are depicted on Figure 18 for a beam with only lower prestressing strands. Figure 19 shows the load forces for a beam with upper and lower prestressing strands.

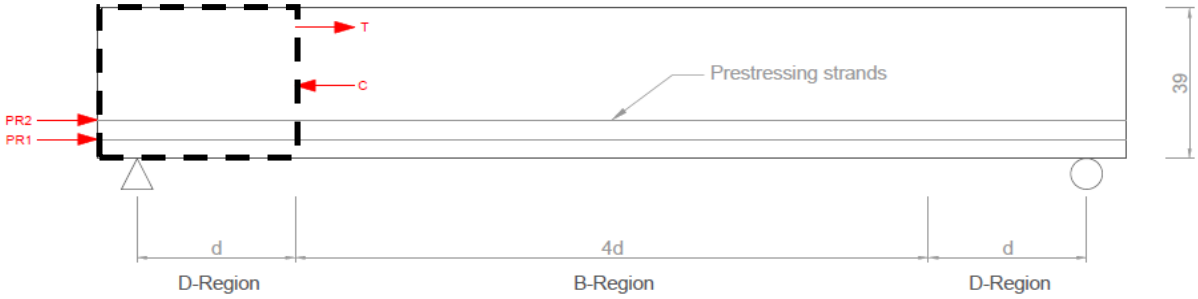

Figure 18 - Step 2: Define the load case for beams with lower prestressing strands

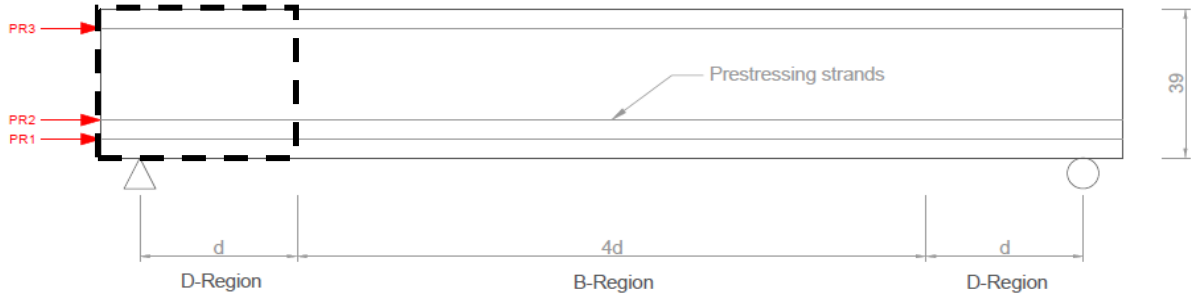

Figure 19 - Step 2: Define the load case for beams with upper and lower prestressing strands

3.5.3 Step 3: Analyse structural component

In this step the acting forces on the B- and D-region interface are determined. These forces are used to further develop the geometry of the strut-and-tie model in the following steps. The location of these forces are determined by using a linear elastic analysis performed in DIANA to show the flow of forces in the beam while prestressing the beam. This non-linear elastic analysis is depicted in Figure 22. Figure 20 and Figure 21 show the location of the B-region/D-region interface. On this interface the reaction forces will be applied. Support reactions are not calculated because no self-weight is considered, by applying the reaction forces of the prestressing strands, the model will still be in equilibrium. If self-weight is considered, there will be reaction forces in the supports. These reaction forces mainly result in compressive stresses which will internally have a positive influence in the anchorage zone of the beam. Due to this positive influence, it is a safe assumption to neglect the self-weight.

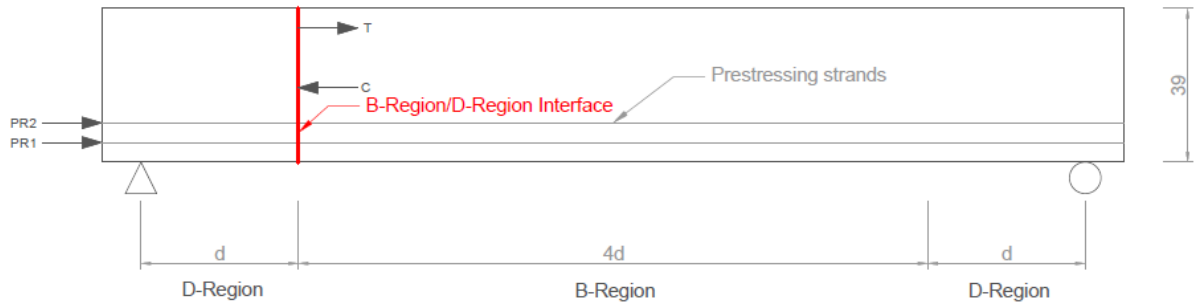

Figure 20 - Boundaries of the D-region for a beam with lower prestressing strands

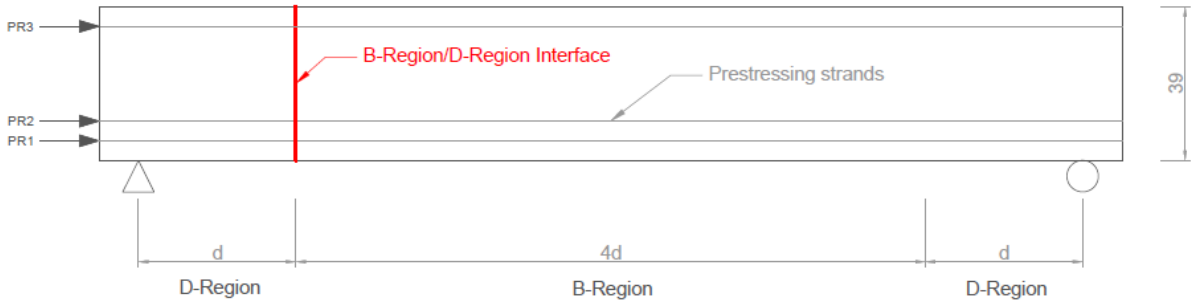

Figure 21 - Boundaries of the D-region for a beam with upper and lower prestressing strands

The vector plot in Figure 22 is derived from previous research of R. Steensels. To better understand these principles it is recommended to read Chapter 5: strut-and-tie model [4]. Based on this vector plot the direction of the horizontal struts and ties can be determined. These directions can also be used to determine the exact location of the reaction forces of the prestressing strands. This will be further explained in step 5.

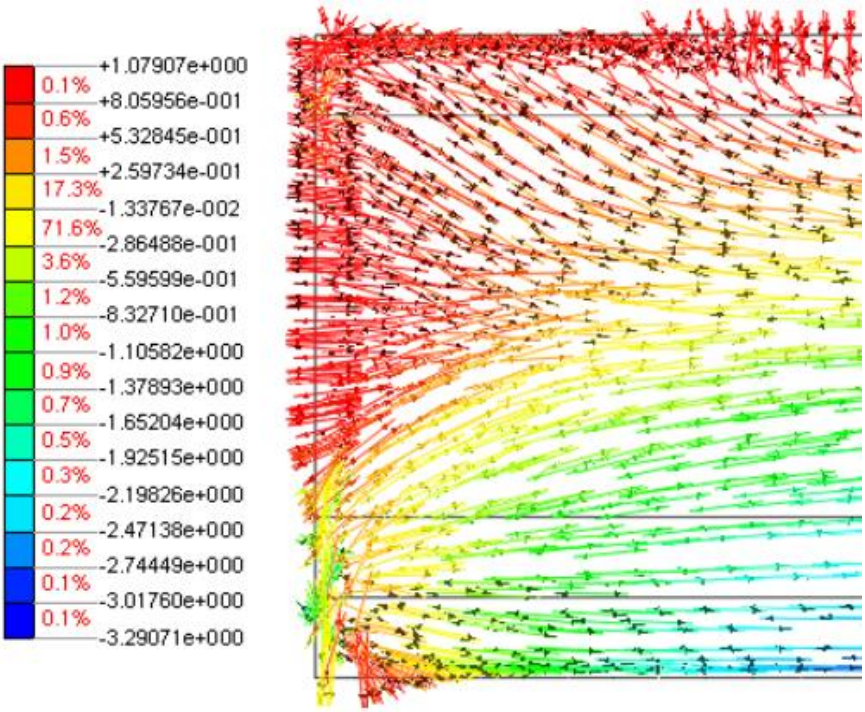

Figure 22 - Vector plots of the second (S2) principle stress of an element with lower and upper prestress strands

3.5.4 Step 4: Adapt the geometry of the structural component (serviceability)

This step is unnecessary for this research. It is used to design the initial beam, in this case an existing beam is used and the dimensions are already fixed. The beams are checked on failure to shear force in this step, the manufacturer has already taken this into account.

3.5.5 Step 5: Design STM

To determine the geometry of the strut-and-tie model there are several options to place the struts, ties and nodes. The first option is to use the location of the applied loads and boundary forces to place the nodes. Another option is to follow the known cracking pattern of the beam. The last option is to perform a non-linear elastic FEA to visualize the flow of forces in the beam and place the struts and ties in the same direction as the flow of forces. R. Steensels opted to use the first option combined with the last option. On the left side of the STM the nodes are placed where the prestressing forces are applied. The right side nodes and the orientation of the struts and ties are based on a vector plot shown in Figure 22.

The ties in the model represent the reinforcement, all the ties are placed on the position of the centroid of the reinforcement. Also the cover of the concrete should be considered. The struts represent the concrete, where mainly compression is present. The horizontal struts at the top should be placed at the optimal height of the strut-and-tie model. The optimum height is achieved by increasing the efficiency of the strut-and-tie model. The final STM for a beam with only lower prestressing strands can be found in red on Figure 23 and for a beam with upper and lower prestressing strands on Figure 24.

For the development of the strut-and-tie model, used in this research, a brief description can be found in section 3.6 or a detailed explanation can be found in the research of R. Steensels [4].

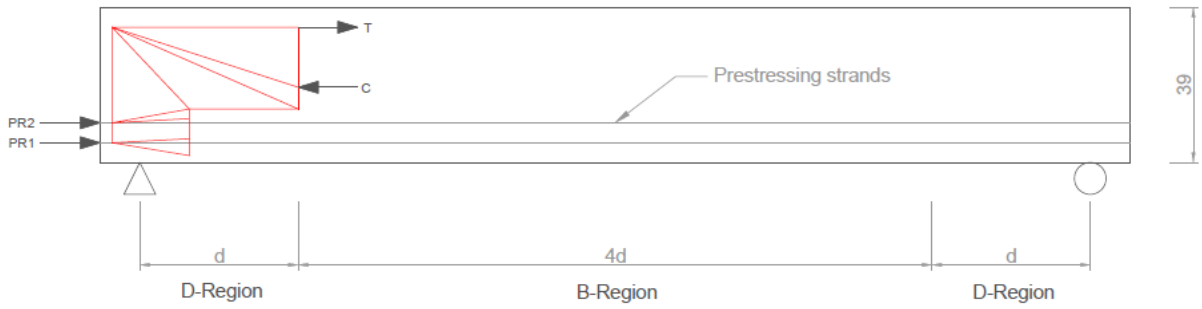

Figure 23 - Step 5: development of the strut and tie model for a beam with lower prestressing strands

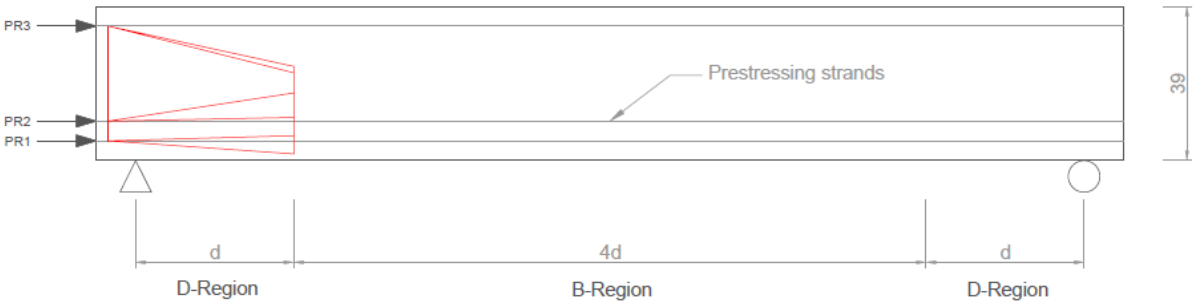

Figure 24 - Step 5: development of the strut and tie model for a beam with upper and lower prestressing strands

3.5.6 Step 6: Determine dimensions of the ties

After modelling the strut-and-tie model in step 5, a numerical or static analysis can be made to determine the forces in each strut and tie. Now the forces of the ties can be used to calculate the reinforcement necessary at the location of each tie. Following equation can be used:

$$A_{st} = \frac{F_u}{\Phi\, f_y} \tag{3.13}$$

Where F_u is the acting force in the tie, f_y the yield strength of steel and Φ is the resistance factor of 0.9 according to AASHTO [13].

3.5.7 Step 7: Perform nodal strength checks

The nodes were not checked in this research, the assumption is made that the nodes will not fail. In a full design the nodes are checked to ensure that the concrete has enough strength without crushing the concrete to withstand the imposed forces. The nodes can be checked as described in Eurocode 2 or in Model Code 2010 as mentioned respectively in paragraph 3.2 and 3.3.

3.6 Principles to design a strut-and-tie model used by R. Steensels

The anchorage zone is a D-region because this place will be disturbed due to the application of the prestress load and due to the support reaction loads. Both discontinuities cause in this region a non-linear distribution of stresses. The traditional beam theory from Bernoulli is not applicable, therefore the use of a strut-and-tie model is required as mentioned in chapter 2 [9]. The length of the D-region is exactly the same length as the transmission length of the beam. The transmission length is the length where a non-linear distribution of stresses occurs, based on St. Venant's principle.

By applying a point load or an abrupt change in geometry or a sudden opening, stress concentrations will occur. St. Venant attaches a grid that will indicate the stress distortions, as shown in Figure 25. The left figure shows the beam at rest while the right figure is pulled sideward. These distorted lines represent the concentrated stresses. According to St. Venant a uniform distribution of stresses is obtained after about a distance the same as the largest dimension of the loaded surface [14].

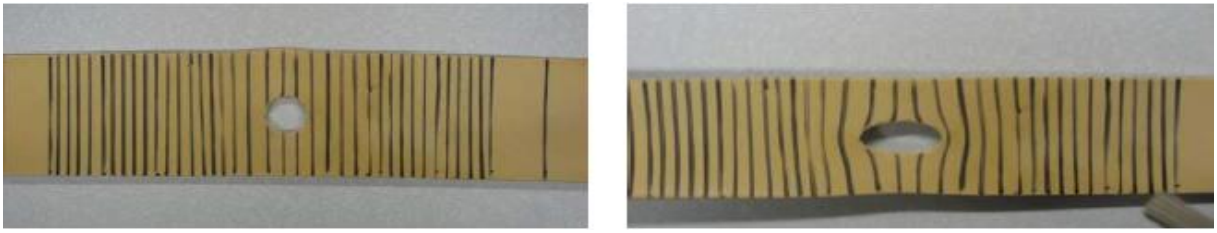

Figure 25 - St. Venant's Principle with a sudden opening [14, p. 1]

3.6.1 Numerical model

To obtain a strut-and-tie model, it is necessary to determine the complex flow of forces through the D-region. The struts and ties need to be placed in the same direction as the elastic flow of forces. There are three tools which are used to determine the orientation of the struts and the ties:

- use the locations of the applied loads and boundary forces;
- use the known crack pattern;
- use a non-linear elastic finite element analysis.

The first tool only determines the starting location of the struts and ties, e.g. the application point of the prestress force. The second tool which uses the flow of the cracking pattern is used to determine the location of the ties in the anchorage zone. These ties are placed perpendicular on the trajectories of these cracks. When using this method, attention must be paid to the correctness of the results because of the many influencing factors. The third tool uses a computer program that uses a linear elastic finite analysis [9]. This analysis shows the flow of forces based on vector plots. The first and the last tool are used together in the model designed by R. Steensels [4].

The final STM lay-out is discussed in the next paragraph. In this paragraph the numerical model is explained which is needed to obtain the strut-and-tie model. The numerical model designed by R. Steensels is based on the FEM software 'DIANA'. In DIANA, the location of the tendons needs to be accounted for. Two situations are possible: only lower reinforcement or reinforcement in the upper and lower flange. The results from DIANA are shown in Figure 26 and Figure 27 which shows the flow of stresses for the principle stresses for respectively a prestressed element with only lower strands and an element with lower and upper strands. In these vector plots will each figure 'a' show the flow of tensile forces, 'b' shows the trajectory of the prestress load and 'c' shows the flow of the compressive stresses [4].

In the case that both the lower and upper flange contains prestress strands, chances are real that these prestressing forces will influence each other. The spalling stresses of each strand group will interact. In a simple linear elastic analysis it is possible to estimate the total spalling stress through a superposition of the spalling stresses from both the lower and upper flanges. In this case, a non-linear analysis is required due to the non-linear concrete material behaviour. A non-linear analysis reflects the reality by taking the crack formation into account and the realistic stress distribution after cracking and concrete softening. The total tensile stress obtained by the superposition is an underestimation of the true tensile stresses. This proves that it is not possible to estimate the total spalling stress through a superposition.

The numerical model contains the transfer of the prestress and also the non-linear material behaviour. The numerical analysis, which is in accordance with Model Code 2010 is conducted in two stages. The first is the assessment of the bond-slip behaviour between concrete and steel. The results of this model will be used as input in the FEM in the second stage where the non-linear material behaviour is implemented [4]. This model can also obtain vector plots of the principle stresses as in the figures below.

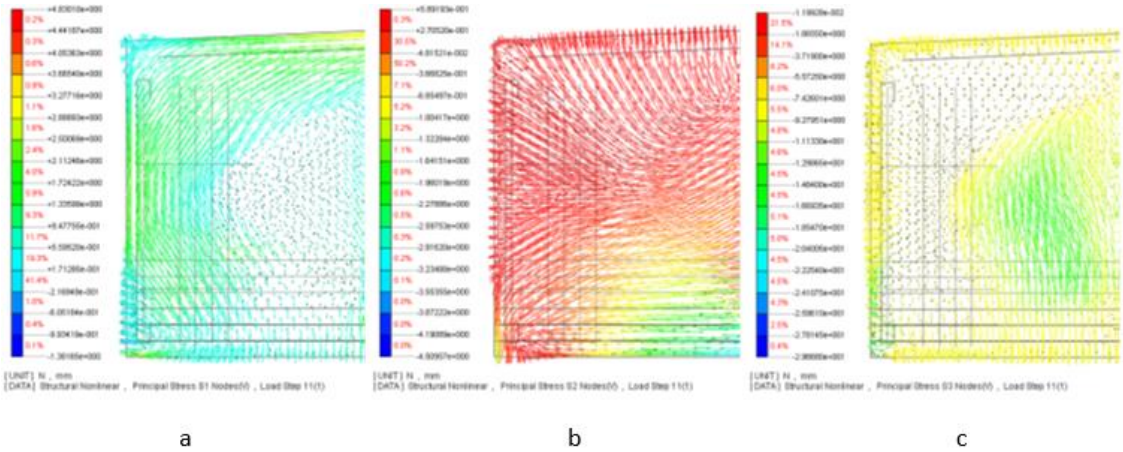

Figure 26 - Vector plots of the principle stresses of an element with only lower prestress reinforcement [4, p. 101]

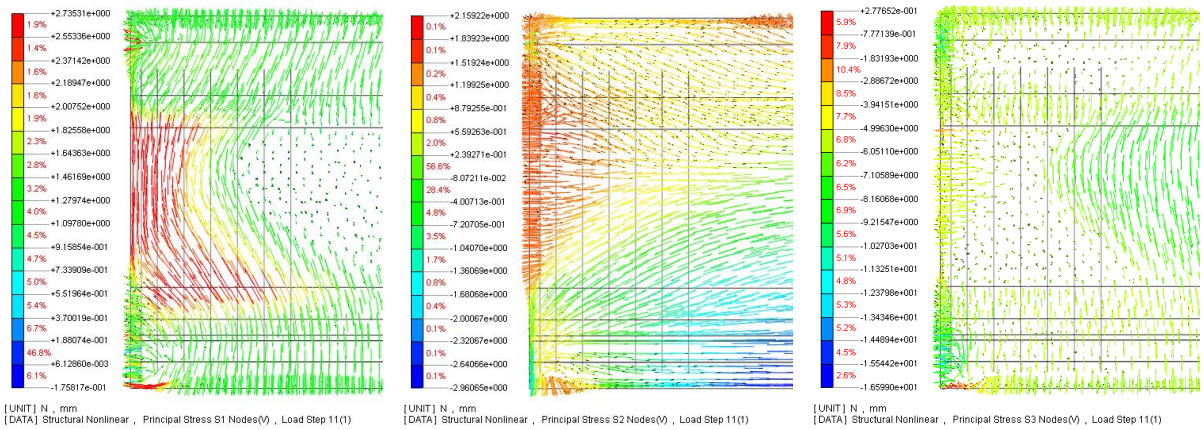

a b c

Figure 27 - Vector plots of the principle stresses of an element with lower and upper prestress reinforcement [4, p. 101]

The vector plots in Figure 26a and Figure 27a illustrates the flow of three principle stresses. Based on the legend, three zones can be indicated with a high value of stresses as depicted in Figure 28a. The first critical zone is a zone with high vertical tensile stresses, called spalling stresses. The second critical zone is the interface between the web and the lower flange. This zone is subject to bursting stresses. The third zone of tensile stresses is located at the top of the end zone of the beam. Tensile stresses in this zone occur when there is sufficient eccentricity. This is the case if there is only lower pretensioned reinforcement. Figure 26b and Figure 27b shows the spreading of the prestress over the transfer length. Tensile forces can be indicated going from the end corners of the beam towards the middle of the beam as can be seen in Figure 28b. Figure 26c and Figure 27c illustrates the largest compressive stresses due to the tendons. These largest compressive stresses are logically located further inward(s) of the element.

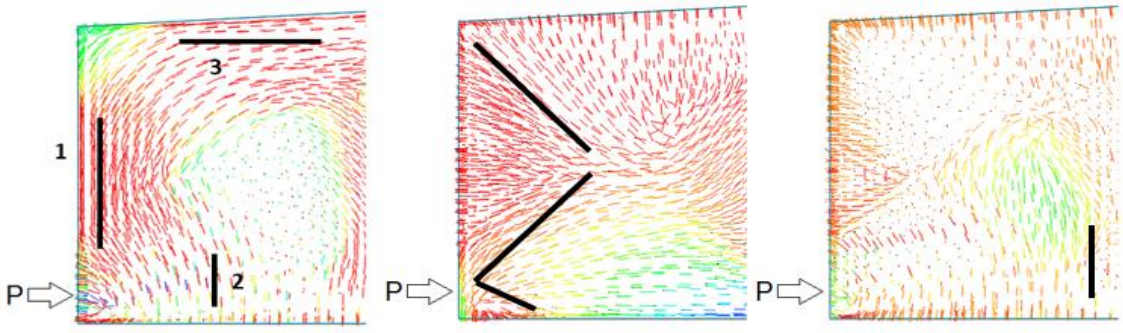

a b c

Figure 28 - Critical tensile regions [4, p. 101]

3.6.2 Strut-and-tie model designed by R. Steensels

The STM designed by R. Steensels et al. [4] is based on the two dimensional vector plots as mentioned before. The general geometry of the STM is designed by using the locations of the applied loads and boundary forces. Based on the principle stress vector plots a general design of the STM is designed as can be seen in Figure 30. This example consists of a beam with only lower prestressed reinforcement that is executed on three levels. Using the first design tool, three nodes can be placed. Further, based on the vector plots, a direction can be given to the struts and ties. The vertical location of the nodes depend on the linear stress state at the transmission length. As can be seen in Figure 29, two struts

depart from each node due the spreading of the prestress load. This effect will be influenced by the geometrical properties of the beam and the location of the prestressed strands. The horizontal locations of the nodes are determined by the transmission length. The length of the struts and ties depend on the length of the transfer length which is discussed in chapter 0.

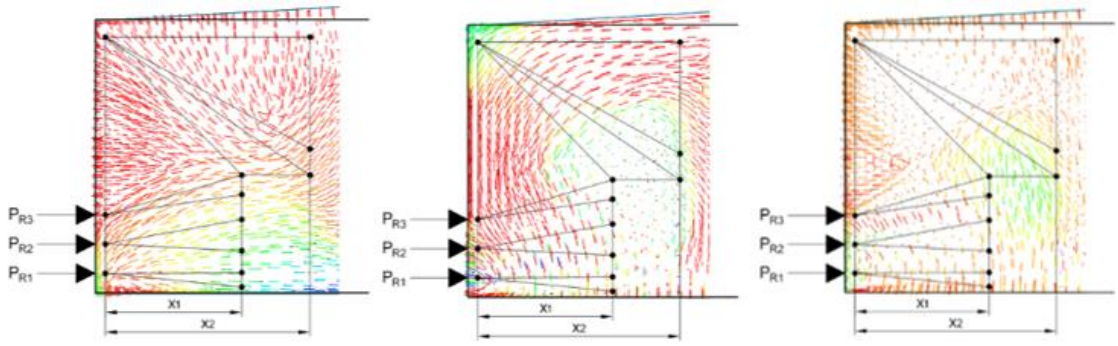

Figure 29 - Design of a STM based on vector plots [4, p. 101]

It is important that the stress trajectories mentioned in section 3.6.1 are reflected in the strut-and-tie model. At the locations of the critical tensile regions needs to be a tie that can counteract the tensile forces. Therefore it is necessary to place a node at the left top corner of the beam which can be connected with surrounding nodes. The diagonal ties are the result of the tensile forces which are presented in Figure 28b. The general design of the STM according to R. Steensels [4] is depicted in Figure 30. The placement of these nodes can be different depending on the designer and the vector plots. This indicates that there is no unique solution for a particular problem. It is possible that one model makes more efficient use of the reinforcement in comparison to another model. In section 7.3, a different version of a strut-and-tie model is proposed to improve the efficiency of the placed reinforcement.

In case of a beam with only lower prestress strands, the prestress force causes an eccentricity. Due to this eccentricity of tendons with force P, an internal linear stress distribution at the B/D-interface arises as shown in Figure 30. This linear stress distribution has a tensile zone in the top of the beam. The resulting moment (M) derives from the tensile stresses and a part of the compressive stresses needs to be equilibrated by a tensile force (T) and compressive force (C).

For elements with both upper and lower prestressed tendons, it is no longer necessary to determine the forces T and C because these are both (almost) eliminated by the prestress of the upper tendons.

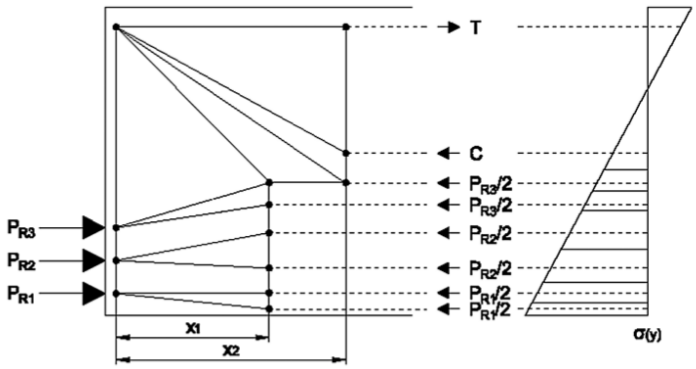

Figure 30 - General design STM according to R. Steensels [4]

4 Different end-zone detailing models through the years

This chapter is to get a better understanding of the development of the modelling of the end-zone of the beam. The most important models that already have been developed are summarized in the next paragraphs. In the first section an experimental determined model by Marshall & Mattock is elaborated. In section 4.2 an American regulation AASHTO is explained. This regulation is a simplified, but conservative version of Marshall & Mattock's empirical equation. Section 4.3 the model of Gergely & Sozen is explained, they made an analysis based on the equilibrium of the cracked section and can determine the spalling force. In the last section Davis & Crispino conducted a numerical campaign and calibrated it with a case study.

4.1 Marshall & Mattock

In the early 60s Marshall & Mattock developed an empirical equation to calculate the required area of end zone reinforcement [15]. The test was based on 25 girders, seven did not crack at all and 14 girders of the 18 remaining showed similar behaviour in the horizontal cracks. By plotting the different measurements the following equation has been found:

$$A_t = 0.021 \frac{P.h}{f_s.l_t} \tag{4.1}$$

Now the amount of stirrup reinforcement can be calculated by equation 4.1. The amount depends on the total prestressing force (P), the design yield strength of the stirrup reinforcement (f_s), the height of the element (h) and the transfer length (l_t)

Marshall & Mattock recommended that the stirrup reinforcement should be evenly distributed over a length equivalent to 20% of the beams' depth, measured from the end part of the beam. For the most efficient crack control, the first stirrup should be placed as close as possible to the end face of the beam as possible. This simple linear relationship has only been proved experimentally for values of h/l_t of up to two. Once increased beyond two, the design equation will tend to become conservative.

4.2 AASHTO

The American Association of State Highway and Transportation Officials (AASHTO) specifications require that a four percent of the prestress force (P) should be taken into account. This four percent prestress force is used as the tensile force that will act at the end zone of the beam. Reinforcement for this tensile force has to be placed as vertical reinforcement in the end zone of the beam [13]. AASHTO also requires that the vertical reinforcement should be placed within a distance from the end of the beam until a depth of h/4. AASHTO suggests a simplified version of the Marshall & Mattock equation. This version assumes that the transfer length is half the height of the element. Equation 4.1 can now be written as equation 4.2.

$$A_t = 0.04 \frac{T}{f_s} \tag{4.2}$$

4.3 Gergely & Sozen

Gergely & Sozen [16] developed a model which is based on writing down the equilibrium of the cracked end zone. When a crack is formed, two sections will remain which are separated by the crack.

In Figure 31 the free body diagram of one of these sections is depicted. The prestress force P together with the internal linear stress distribution at the transmission length will induce a moment M. This needs to be equilibrated by a tensile force T taken by the reinforcement and a compressive force C taken by the concrete [17]. These forces will act perpendicular on the crack. Gergely and Sozen propose that the leverage arm between the internal forces is the height of the element.

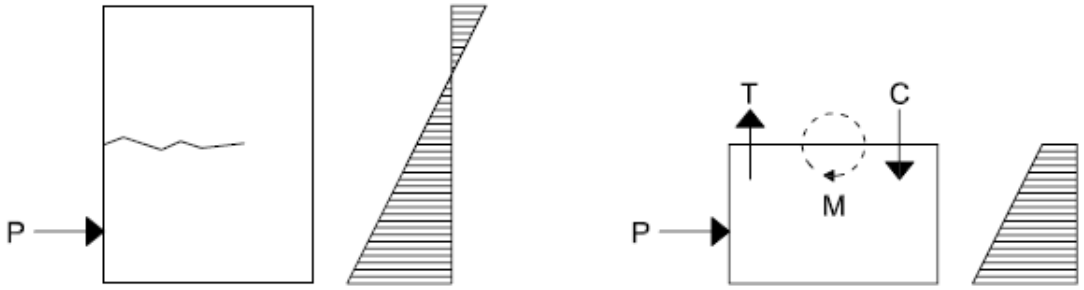

Figure 31 - Gergely-Sozen anchorage zone design [4, p. 19]

Gergely and Sozen do not only calculate the maximum spalling force in the end zone, they also calculate the height where the first crack is going to appear. The first crack will appear at the location of the maximum moment. A more eccentric prestressing force P will result in a higher unbalanced moment M, which will result in a higher spalling force.

4.4 Davis & Crispino

4.4.1 Davis

Davis et al. [4] conducted a numerical model which is calibrated with a case study from field observation of an actual bridge. This STM is made up of two strut-and-tie models. The first model is built up to limit the cracks at the bulb to web interface. The second model is built up to limit the diagonal cracks in the web of the beam. These models are solved separately.

As Gergely and Sozen did, Davis uses the division of the anchorage zone in two sections at the height of the spalling crack. The external force of the lower tendon is computed by multiplying the stress with the reinforcement area. The same is done with the upper area. After equilibrating the moment in the lower section with the upper section, the exact position of the internal forces can be computed at a distance h from the end zone of the beam. The two strut-and-tie models and the internal forces can be seen in Figure 32. In the upper model the tension force acts uniformly over a length of 3/4h from the end of the beam and in the lower model, the tension force acts uniformly over a length of h/4 from the end of the beam [6].

Davis et al. concluded from the parametric study that four percent of the total prestress force is a good directive for the requirement reinforcement in the vertical direction in the anchorage zone of short beams. In larger beams, five percent will be a better directive. To conclude the case study, they determine that a group of closely spaced vertical reinforcement near to the beam end cannot control the diagonal cracks. Also, the stiffness of the vertical stirrups is related to the crack widths.

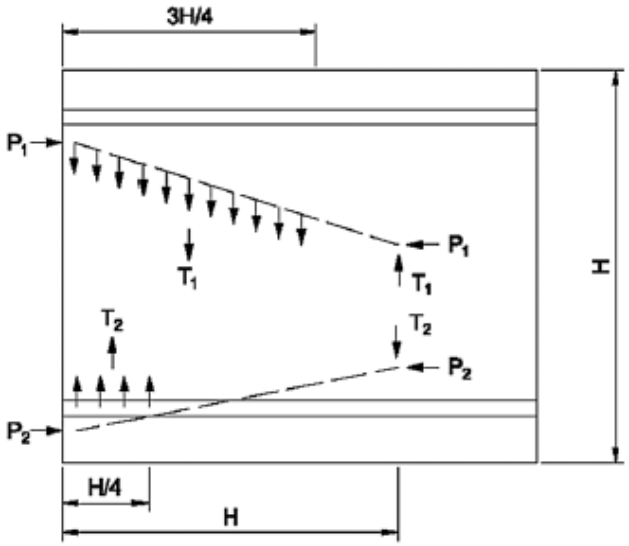

Figure 32 - STM according to Davis et al. [6, p. 8]

4.4.2 Crispino

As concluded in Davis' research, the diagonal cracks cannot be controlled in case of a group of closely spaced vertical stirrups. Thus, Crispino [6] improved the model by a better distribution of the vertical reinforcement. Due to these stirrups, there is a link between lower and upper strut-and-tie model as can be seen in Figure 33. T_1 and T_2 are equal because the angles in the ties are developed in a specific manner and are calculated as presented in equation 4.3:

$$T_1 = T_2 = \frac{8 * P_1 * y}{7 * H} \tag{4.3}$$

This model was developed to determine the required vertical reinforcement area as obtained in the fundamental theory used in STM. The model is called a true double-tie STM. A parametric study claims that the required reinforcement in the area within H/4 is about the same as between H/4 and 3H/4.

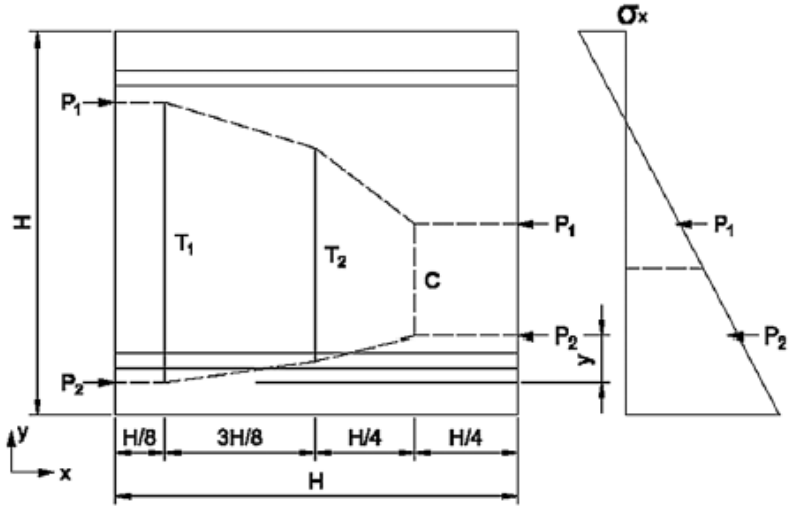

Figure 33 - STM according to Crispino et al. [6, p. 15]

5 Modelling the anchorage zone of pretensioned elements

This chapter will shortly explain the underlying concepts of how the confinement of the concrete and the steel are detailed. A two-staged modelling approach is presented. In the first stage, a small-sized beam with only one prestressing strand is modelled, where the equivalent strand confinement is used. Also the material properties of the full-scale beam are used, thereafter the bond-slip behaviour can be evaluated. Hence, the bond-slip behaviour together with the transfer length of the prestressing strands can be determined by using a simple numerical model. Next, in the second stage, this bond-slip behaviour is implemented in a full-scale finite element model to calculate the anchorage zone stress field [4]. Finally, when this behaviour is fully modelled and verified, it can be used as a realistic input to determine the stress trajectories on which the strut-and-tie model is based.

5.1 Confinement model

The bond behaviour is influenced by several different parameters: geometric, material and mechanical parameters. Most of these parameters are contained within the confinement of the prestress strand. This is achieved by analysing the thick-walled cylinder model. The non-linear softening behaviour of the concrete and the loss of confinement due to the formation of splitting cracks around the tendons can now be included.

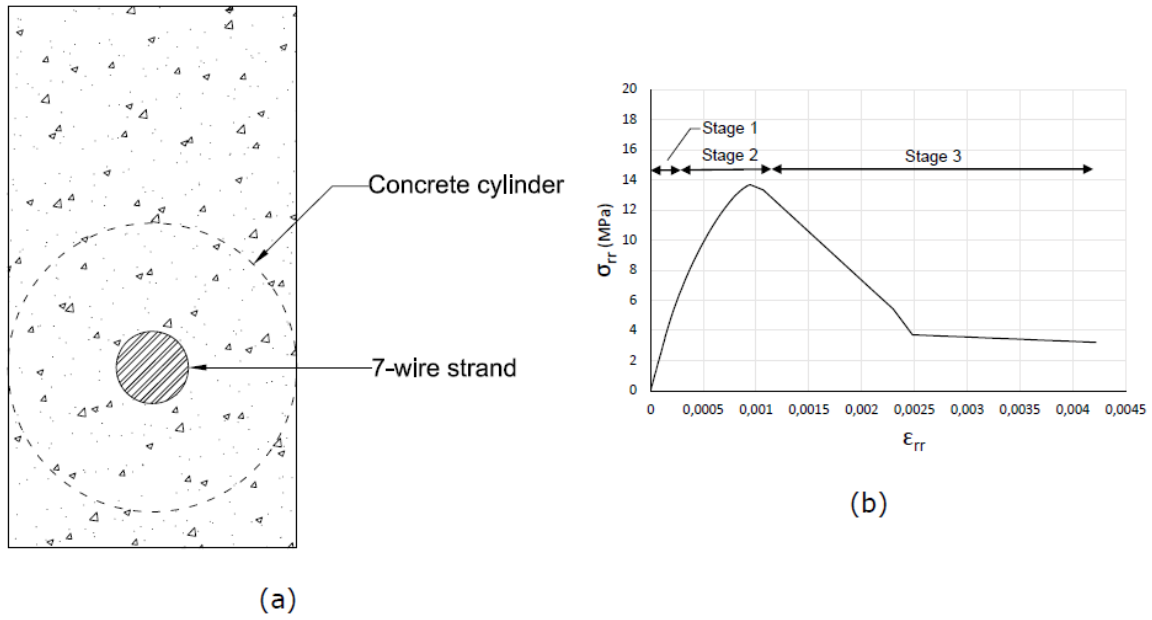

Figure 34 - Thick walled cylinder model: geometry (a) and different stress stages (b) [4, p. 32]

Figure 34a shows a cross section of a rectangular beam with a seven-wire strand as the inner cylinder and the outer cylinder is the effective concrete cover. When analysing this model, shown in Figure 34b, three stages can be identified. The first stage is the linear elastic behaviour of the concrete cylinder. In the second stage micro-cracking will occur followed by the cracking front propagating to the outer radius of the concrete cylinder. In the last stage, the crack width increases, this results in further softening of the concrete. This behaviour will be taken into account.

Now the bond-slip relation can be deducted. According to R. Steensels [4], the following equation gives an expression of the full bond-slip behaviour at the steel-concrete interface. The total contribution of the bond-slip, $\epsilon_{rr,tot}(\delta)$ is respectively the wedge effect, the 'lack-of-fit' effect and the pitch effect to the total radial strain at the interface.

$$\epsilon_{rr,tot}(\delta) = (C_v v_s + C_{mech})\frac{\delta}{l_t} \tag{5.1}$$

With C_v and C_{mech} calibration constants, v_s is the steel Poisson's ratio, l_t is the transfer length and δ the slip. An experimental campaign calibrated these constants, these calibrated values can be found in Table 3.2. It should be noted that these constants are only valid for 7-wired prestressing strands [4].

Table 2 – Calibrated constants for the bond-slip model [4, p. 39]

Calibration constant	Value
C_v	1
C_{mech}	0,20

5.1.1 FEA: stage I

A numerical analysis of the pretensioned beam is conducted using DIANA. The bond-slip behaviour as mentioned before will be implemented in the material behaviour of the ties. Linear elastic material properties of steel and concrete are used. Since the constitutive law of the thick-walled cylinder model is included in the material behaviour, the influence of the radial expansion of the strand, the likely to occur splitting cracks and the softening behaviour on the confining action of the concrete cover and thus on the bond strength don't have to be calculated separately but are already included.

The prestress force on the beam is modelled as several prestressing forces acting on the end-zone of the beam. This force will gradually be transferred from the prestressing strands to the surrounding concrete at the steel-concrete interface.

In Figure 35 an iterative procedure to find the correct bond-slip relation and the transfer length is depicted. In the first iteration step, the transfer length has to be guessed. According to AASHTO regulations the transfer length is 60 times the diameter of the 7-wired strand, this initial guess will make sure the iteration will only take 5 to 10 iteration steps. From the transfer length, the bond-slip behaviour can be determined. This relation is implemented in the FEM and the analysis will be executed. These computations will return the strain field of the beam and a new transfer length is calculated regarding to the 95% Averaged Maximum Strain method. If this transfer length does not match the transfer length calculated previously, a new bond-slip relation will be calculated using the new transfer length and the process repeats itself.

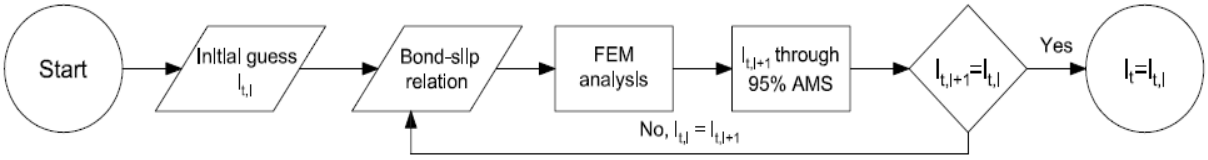

Figure 35 - Flowchart of the bond-slip model [4, p. 36]

When multiple strands are used, an effective concrete cover will be calculated to use the thick-walled cylinder model. This effective concrete cover will represent all strands throughout the cross-section. For the determination of the bond-slip behaviour, the model with only one prestressing strand with a specified concrete cover C_{eff} is used. By using this effective concrete cover, a small cross section with an equivalent confinement behaviour is achieved to analyse the bond-slip behaviour of the original section more efficiently.

An evaluation of this model was conducted by verifying the transfer length of this bond-slip model with the experimental values of Mitchell et al. [18] and Oh et al [19]. Together 22 beams were tested, comparing the transfer length from these experimental beams with the bond-slip model resulted in a good agreement between the bond-slip model and the experiment. An error of 8% is obtained. This error could be due to the dynamic effects that will happen at the cutting end of the beam. These dynamic effects will result in a higher value of the transfer length. Also, after cutting the prestressing strands, the strands will move to the anchor point while also resulting in prestress release on that side.

5.1.2 FEA: stage II

In the second stage the bond-slip model which is calibrated in the previous stage will be used to calculate the non-linear stress distribution. Also it will calculate the positions where cracking in the anchorage zone of the prestressed members may occur.

Two different loading phases can be seen in the full beam model. The first phase will apply the self-weight, while the second phase will apply all the prestress loads in the right sequence depending on the way of releasing or cutting the strands. To take into account the self-weight and to design the upward curvature occurring while prestressing the bottom part of the girder, the casting bed is modelled by using rigid components and providing a non-linear interface between the girder and the casting bed. To model the bursting and spalling stresses on the end zone of the beam, the non-linear material behaviour of concrete is accounted for. Splitting cracks were also taken into account in this model. Also the loss of confinement due to these splitting cracks are included in the bond-slip behaviour used by the thick-walled cylinder model as discussed in the first stage. A realistic model has been set up.

5.2 Validation of the model

This model has been validated on the global behaviour of the girder by comparing the axial strains of the numerical model with the theoretically calculated values based on normal beam theory. The local behaviour is validated using strain data of the tendons and passive end-zone reinforcement collected by O'callaghan [20]. On both levels the results show a good agreement for all the different tested girders. As a second comparison, the passive reinforcement of the anchorage zone is compared to the experimental data and the numerical data. In general these strain distributions compare well but some discrepancies can be found. Nevertheless, it can be concluded that despite some flaws, this model is a very good approximation to calculate the passive reinforcement. The greatest advantage is the level of accuracy, only using the bond-slip analysis in stage I and the anchorage zone analysis in stage II. Which can be completely calculated with input data known at the design stage of the element, no experimental input is necessary.

6 Safety factors & losses of prestress

This chapter is divided in three general parts. In the first paragraph the need for safety factors in the design of constructional elements is explained. The next paragraph explains all prestress losses and will indicate which losses are relevant to this research. Also one reduction factor for the prestress force is given in favourable conditions and a safety factor for prestress forces in unfavourable conditions. The last paragraph deals with the implementation of these safety factors in the numerical model used to design the anchorage zone of the beams.

6.1 Safety factors

Several safety factors are used to design a beam [21]. First of all the material properties will statistically have a normal distribution of its resistance and therefore will be divided by each specific safety factor. The resistance of the materials are underestimated to reach a safe approximation. For concrete the material safety factor $\gamma_c = 1,5$ and for steel $\gamma_s = 1,15$ is used. The forces acting on the structure will be overestimated, so higher forces will be used in the design. Safety factors for permanent and variable loads are respectively 1,35 and 1,5. The forces are multiplied by these safety factors. The safety factor for prestressing forces is 1,0 instead of 1,35 because the load is favourable in general structural analysis, like mentioned in Eurocode 0 [22]. But to calculate the vertical reinforcement at the end of the beam a factor of 1,3 has to be used because the pretensioning is unfavourable. This pretensioning will cause cracks to develop. In the end zone the pretensioning is disadvantageous, the necessary losses will be taken into account.

For a complete design of the beam all these safety factors should be taken into account. In this research only the reinforcement in the end zone of the beam is designed, so only the prestressing safety factors should be taken into account. In the next paragraph an attempt is made to determine one single prestress-loss factor.

6.2 Prestress losses

Prestress loss is the difference between the initial prestress and the effective prestress that remains in a tendon. During the prestressing procedure several losses will occur. Some of the losses are neglectable, some are irrelevant to this research but others are worth taking into account. The losses of prestress can be classified into two types which also can be subdivided into three types each [23]. Figure 36 shows an overview of the different losses.

The first type is an immediate loss that occurs after flame cutting the tendon or releasing the jack, while the prestress is being transferred to the concrete. Immediate losses are important to this research because the horizontal cracks in the end-zone will occur in the first hours after the pretensioning. These short-term losses can also be classified into three types. Each type will be clarified in the paragraphs below.

The second type is a time dependent loss that occurs during the service life of the structure. These long-term losses can also be classified into two types. Each type will be clarified in the paragraphs below. These losses are considered less important because the horizontal cracks will be formed in the first hours after pretensioning.

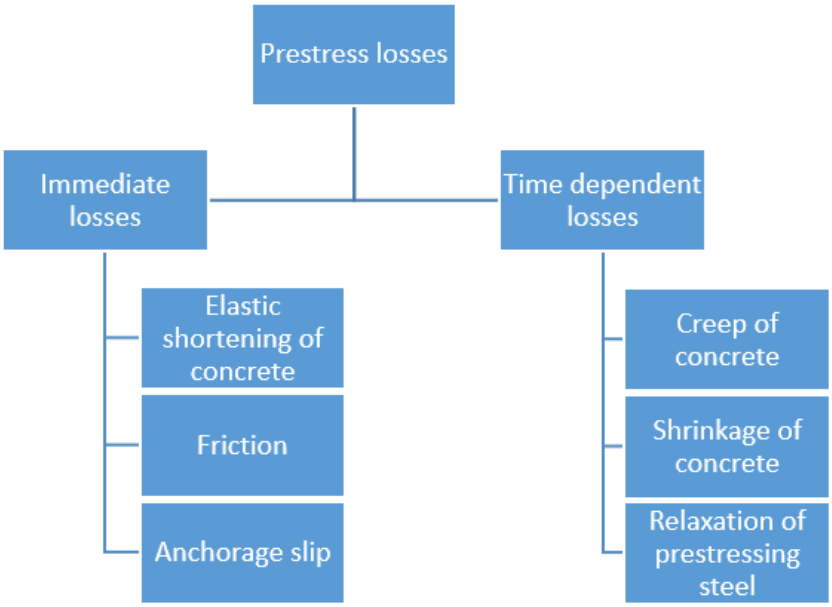

Figure 36 - Prestress losses [23, p. 3]

6.2.1 Immediate losses of prestressing

Losses due to the instantaneous deformation of concrete

Due to the axial forces on the concrete by the tendons, a deformation of the concrete is obtained. Because the concrete's length will get smaller, a smaller strain of the tendons is achieved which will result in a loss of prestressing strength. After cutting the tendons, a deformation of the concrete will occur. This loss ΔP_{el} can be taken into account according to Eurocode 2 as follows [12]:

$$\Delta P_{el} = A_p . E_p . \sum \left[\frac{j . \Delta\sigma_0(t)}{E_{cm}(t)} \right] \tag{6.1}$$

With A_p and E_p respectively the cross section and the young's modulus of the tendon. E_{cm} is the mean young's modulus of the concrete at time t. $\Delta\sigma_0(t)$ is the variation of stress at the centroid of the prestressing strands, calculated at time t. j is equal to (n-1)/2n where n is the amount of identical tendons successfully prestressed. When more tendons are used, j will approximate 0,5.

N. Krishna Raju suggests a simpler linear method [24]:

$$Percentage\ loss\ of\ stress\ in\ steel = \frac{\alpha_c f_c}{f_s} \tag{6.2}$$

$$\alpha_c = \frac{E_s}{E_c} \tag{6.3}$$

With E_s and E_c respectively the young's modulus of steel and concrete and f_c, f_s are respectively the tensile stresses in the concrete and steel. This simplified calculation of N. Krishna Raju is used to determine the losses due to the instantaneous deformation of the concrete in the numerical model used in this research.

Friction

Friction loss is a loss that occurs in case of a curved tendon. Curved tendons are mainly used at post-tensioned beams. Due to the curved ducts, there will be losses due to friction between the tendon and the duct. Due to this friction it is not possible to transmit the full prestressing stress. In addition, friction losses also consist of the loss as a result of the wobble-effect. This effect is about that the elongation has to overcome the curvature of the tendon. Pretensioned beams usually have a linear tendon because of its simple design. This means that no account should be taken for the friction losses in a pretensioned beam because there is no concrete around the tendon while stressing the tendons [23].

Losses at anchorage

When the tendon is tensioned and the jack is released or the tendon gets flame cut, the tendon will slip over a small distance before the tendon is firmly attached to the concrete. The amount of slip depends on the type of anchorage and the stress in the tendon. Eurocode 2 mentions that the losses of the wedge draw-in of the anchorage should be taken into account. Both during the anchoring and after tensioning the strands and also due to the deformation of the anchorage itself. No calculation of the anchorage losses could be found in Eurocode 2. N. Krishna Raju suggests following method [24]:

$$\frac{PL}{AE_s} = \Delta = slip \tag{6.4}$$

$$\frac{P}{A} = \frac{E_s \Delta}{L} = Loss\ of\ stress\ due\ to\ anchorage\ slip \tag{6.5}$$

Δ = slip of anchorage in mm
L = Length of the tendon in mm
A = Cross-sectional area of the tendon in mm²
E_s = Modulus of elasticity of steel in N/mm²
P = the total prestressing force in the tendon in N

A calculation of the slip is possible as mentioned in equation 6.4, but an experimental determination of the slip will give a better indication of the slip, because equation 6.4 and 6.5 are linear simplifications. In real, the tendon will also rotate around its axis, which will result in additional torsional friction. Since the loss of the prestressing stress is a certain amount of shortening, the percentage loss is higher for short members than for long ones.

6.2.2 Time dependent losses of prestress for pretensioning and posttensioning

The highest stresses are obtained in the beginning of the prestressing, time dependent losses will decrease the stresses over time. In this research time dependent losses can be neglected, this is a safe assumption because the horizontal cracks will occur in the first hours after prestressing.

By reducing the strain which happens because of the creep and shrinkage of the concrete under permanent loads and also a reduction of stresses in steel due to the relaxation of steel in tension occurs [12]. These losses can be calculated with a simplified formula to evaluate the time dependent losses at location x under a permanent load:

$$\Delta P = A_P \Delta\sigma = A_P \frac{\varepsilon_{cs} E_P + 0{,}8\Delta\sigma_{pr} + \frac{E_P}{E_{cm}}\varphi(t,t_0)\sigma_{OP}}{1 + \frac{E_P}{E_{cm}}\frac{A_P}{A_c}\left(1 + \frac{A_c}{I_c} z_{cp}^2\right)[1 + 0{,}8\varphi(t,t_0)]} \quad (6.6)$$

Also MC1990 [25] mentions the time-dependent losses of prestressing. Due to the creep and shrinkage of the concrete, a smaller strain of the steel is obtained, which will result in a smaller prestressing stress. But on the contrary to Eurocode 2, MC1990 has not given an equation to determine those losses.

6.2.3 Total losses allowed for design

The loss of prestress depends on several factors: the properties of concrete and steel, geometric properties, method of curing, amount of prestress and the method of prestressing. It is very difficult to generalize a percentage of loss. However, typical percentages losses of stress under normal conditions are shown in Table 3.

Table 3 – Percentage loss of stress [24, p. 132]

Type of loss	Percentage loss of stress (%)	
	Pretensioning	Post-tensioning
Elastic shortening and bending of concrete	4	1
Creep of concrete	6	5
Shrinkage of concrete	7	6
Creep in steel	8	8
Total	**25**	**20**

N. Raju [24] mentions that in these recommendations it is assumed that temporary overstressing is done to reduce relaxation, and to compensate for friction and anchorage losses.

$$Reduction\ factor\ for\ loss\ of\ prestress = \eta = \frac{f_{pe}}{f_{pi}}$$

$$f_{pe} = effective\ stress\ in\ tendons\ after\ losses$$

$$f_{pi} = stress\ in\ tendons\ at\ transfer$$

According to N. Krishna Raju [24] a value of η = 0,75 for pretensioning is a safe assumption to design a beam. This loss of 25% is obtained by adding all the different prestressing losses presented in Table 3. But in this research, the shrinkage of concrete and the creep in steel and concrete can be neglected. Anchorage losses and relaxation losses are not included. Different reduction factors can be found for different girders and beams because the losses are dependent on the geometry of the beam and the quantity of reinforcement, etc. To design the anchorage zone it is important to overestimate the prestressing forces. These prestressing forces have a negative influence to the durability of the beam. A safety factor of 1,3 is recommended, which is used for prestressing forces that are unfavourable according to Eurocode 0 [22].

6.3 Implementation of safety factors due to the pretensioning losses

As a simplification, certain abbreviations will be used when talking about the different beams. For example R400L stands for an R400 beam with only Lower reinforcement and a R400UL beam stands for a R400 beam with Upper and Lower reinforcement. The properties of the different beams can be found in section 7.1.

When a certain amount of elongation is made to a specified amount of prestressing strands, the exact prestressing force can be calculated. When releasing the jack or flame cutting the prestressing strands several losses will occur as explained in previous parts of this chapter. To implement a safety factor for these losses, the calculated reinforcement has to be the same as before the prestressing losses were calculated. First, the relation between the prestress losses and the change in lever arm L1 with upper and lower reinforcement is explained in section 6.3.1. Secondly, this relation is also discussed for beams with only lower reinforcement in section 6.3.2. In the last part of this chapter a comparison between both these beams is made.

6.3.1 Upper and lower reinforcement

In Figure 37 the STM is depicted with the axial forces in the struts and ties where the lever arm L1 is the horizontal length of the STM. The green lines, shown in Figure 37, indicate the compressive forces, while the red lines indicate the tensile forces. When using upper and lower reinforcement, only L1 is used.

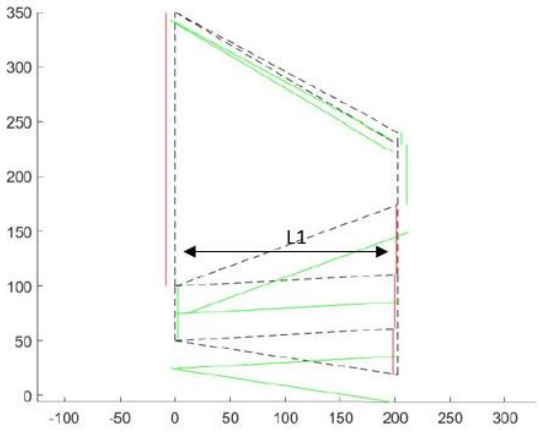

Figure 37 - STM of upper and lower reinforced beam

When a certain amount of prestress loss is calculated in the model, a certain relation between the percentage prestress loss and the fraction of the transmission length can determine the reduction of L1 that will result in the same amount of reinforcement as without the prestress loss. When prestress losses are subtracted from the initial prestress force, a lower amount of reinforcement will be calculated. This is not desirable, the same amount of reinforcement as without these losses should be obtained for safety reasons. The initial model has been programmed without any safety factors. Taking into account the prestress losses will result in smaller tensile stresses in the anchorage zone of the beam. By doing so, not enough reinforcement will be placed. This can be avoided by calculating these losses in advance and adapting the leverage arm to obtain the same internal forces in the struts and ties as without these losses. And if the internal forces are the same as before, the reinforcement will also be sufficient. Without any losses L1 amounts 0,33 times the transmission length. As can be seen in Figure 38, a linear relation between the percentage prestress loss and the lever arm L1 is found to obtain the same reinforcement is found for a R400UL beam.

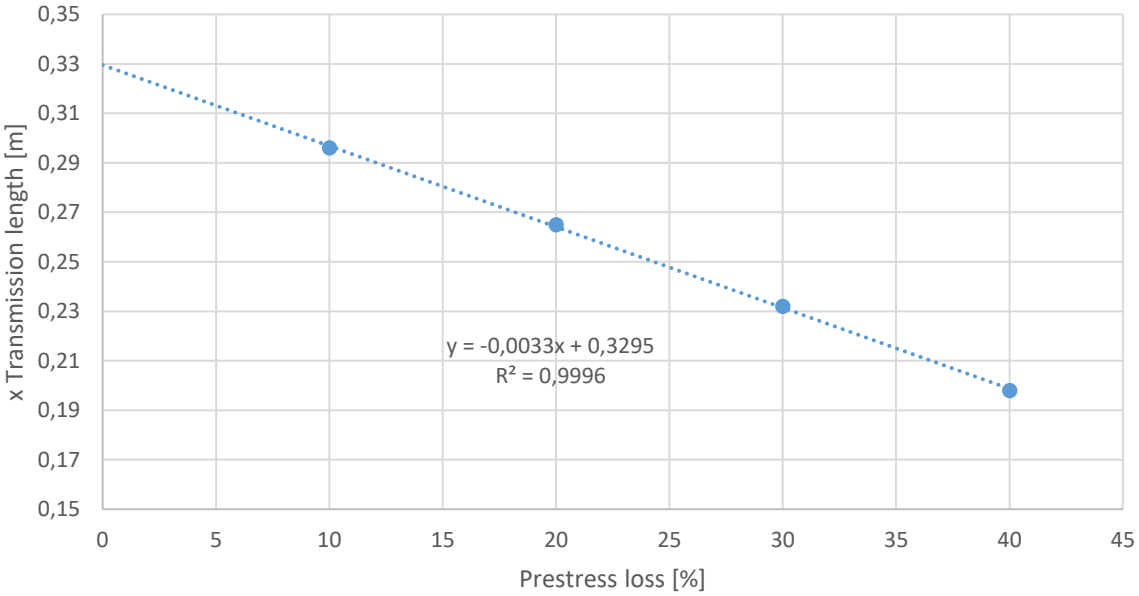

Figure 38 - The percentage prestress losses in function of the L1 lever arm (R400UL)

Figure 39 shows the same linear relation when an I700UL profile is tested. This will make it possible to take into account a safety factor for the prestress losses for any beam with upper and lower prestressing strands.

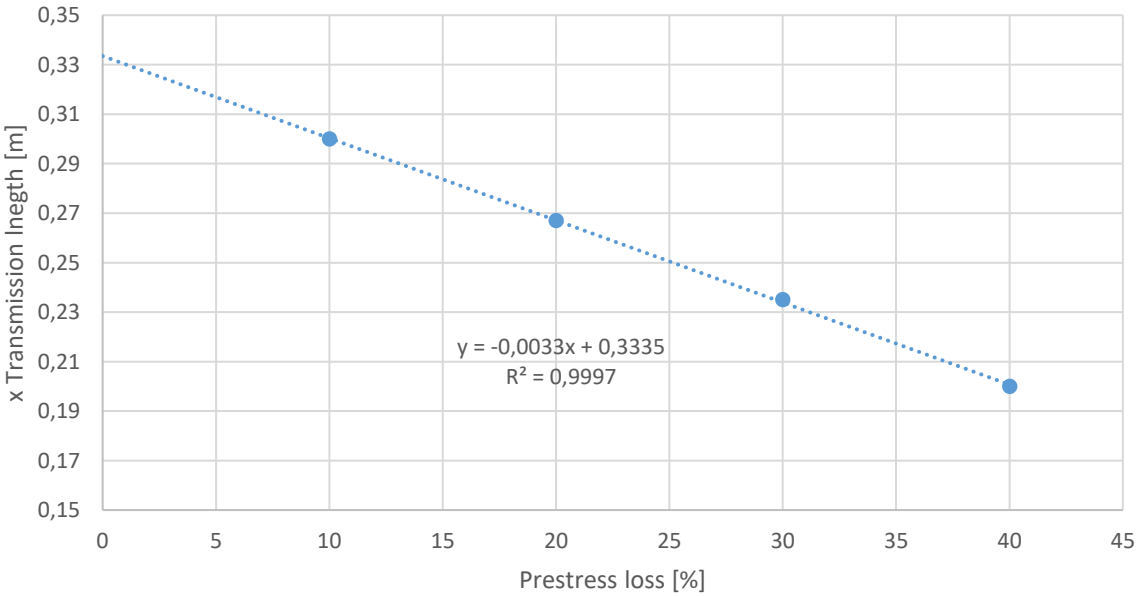

Figure 39 - The percentage prestress losses in function of the L1 lever arm (I700UL)

Figure 40 depicts the percentage loss of prestress in function of the percentage reduction of prestress loss relative to the initial prestress when no loss is applied. When a prestress loss of 10% is experimentally determined, a higher percentage reduction than the prestress loss of 10% of L1 is necessary to maintain the same internal forces, as can be seen in Figure 40. When a 40% prestress loss is applied, there has to be a 66,7% change in the length of L1. This relation can be described as a second degree polynomial.

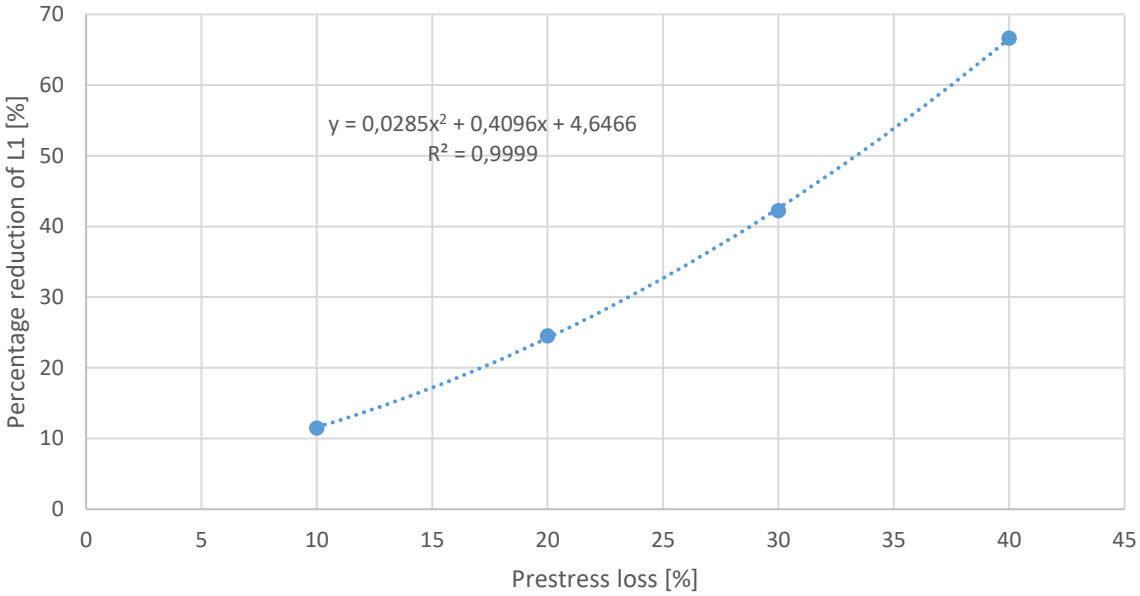

Figure 40 - Percentage of prestress loss in function of the percentage of reduction of L1 for the R400UL

6.3.2 Lower reinforcement

When only using lower reinforcement also a L2 is defined as depicted in Figure 41. In Figure 41 the green lines are the compressive forces for the related truss, while the red lines are the tensile forces. This L2 for beams with only lower reinforcement is used because this design will better follow the flow of forces on the vector plots. Looking back, if L2 was left out and all the nodes were placed at a horizontal distance L1 the results would have been the same, this is confirmed in this section.

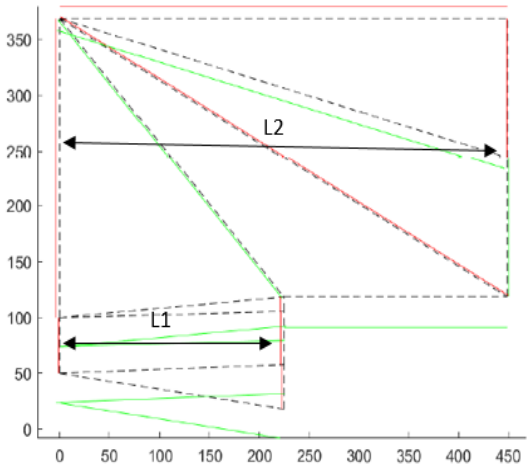

Figure 41 - STM of lower reinforced beam

When the same reinforcement is desired as before the prestress losses, it means that the forces in each tie of the STM has to remain the same. Figure 42 shows the relation between the percentage prestress loss and the corresponding fraction of the transmission length to obtain the same internal forces. As can be seen in Figure 42 the same linear relation is found as in section 6.3.1 for the R400UL beam with only lower reinforcement and no upper reinforcement. During this experimental campaign it also came forward that changing L2 which is used in the model when only lower reinforcement is used, as described beneath, no influence can be found by changing the value of L2. Only by changing L1 the internal forces will change.

Table 4 also confirms that changing L2 has no influence on the internal forces of the strut-and-tie model. The trusses used to compare in Table 4 are shown on Figure 44 in red. Truss number 2 are the spalling forces, whilst the other trusses are the bursting forces. L1 has been fixed to 0,33 Lm, while L2 changes from 0,66Lm to 0,9Lm. In the first column the numbers of the different trusses corresponding to the bursting parts of the STM are displayed. In the second column of Table 4 the internal force of the corresponding truss without any prestress losses is shown. The third column of this table shows the internal force with the prestress losses taken into account and also the influence of changing the lever arm L2. But when looking further in the table when L2 changes, these forces with the loss taken into account shows no variation. The last column in Table 4 is the ratio of the column 'Tensile force without loss' and 'Tensile force with loss'.

Figure 43 depicts the percentage loss of prestress in function of the percentage reduction of prestress loss relative to the initial prestress when no loss is applied. Again a second degree polynomial is obtained. Exactly the same relation has been found as for beams with upper and lower reinforcement as mentioned in section 6.3.1.

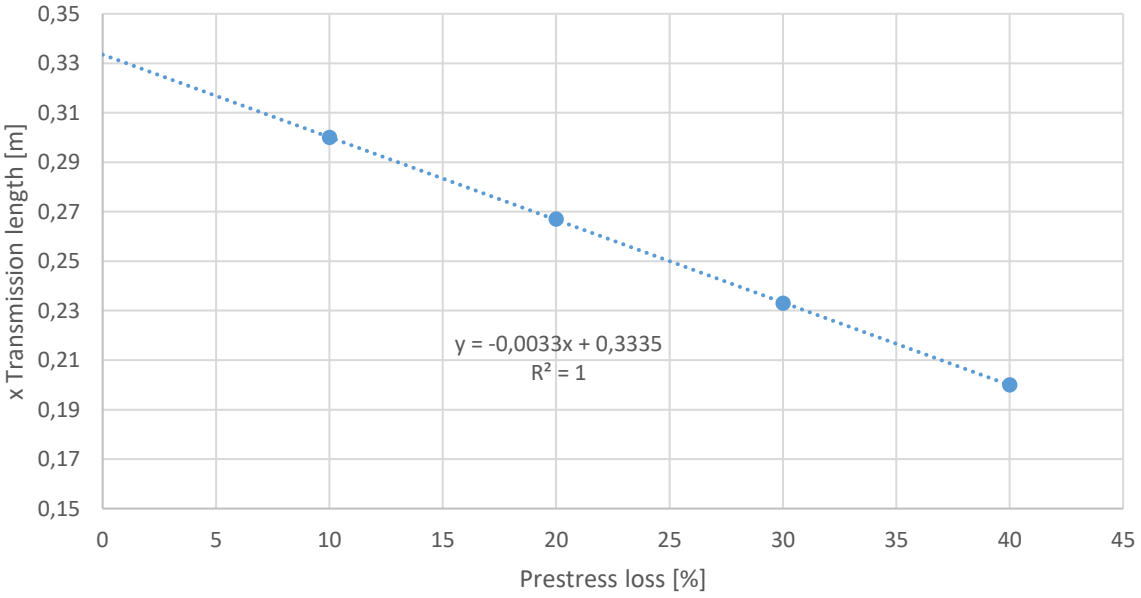

Figure 42 - The percentage prestress losses in function of the L1 lever arm (R400L)

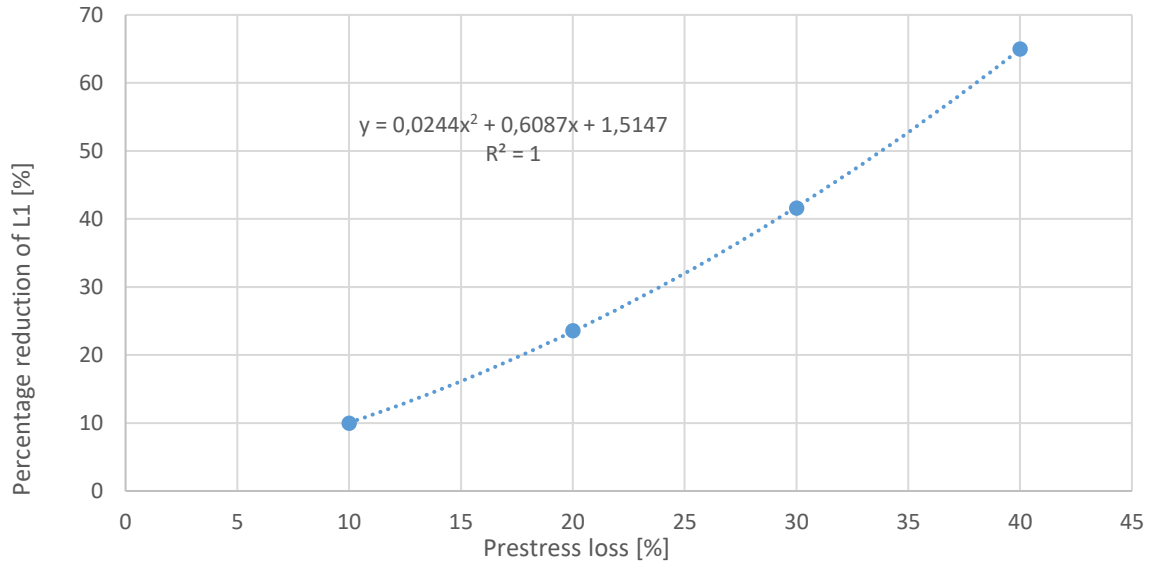

Figure 43 - Percentage of prestress loss in function of the percentage of reduction of L1 for beam R400L

Table 4 – Changing L2 and keeping L1 constant

L1 = 0,33 Lm L2 = 0,66 Lm			
Truss number	Tensile force without loss [N]	Tensile force with loss [N]	Ratio
2	58718	52847	1,111094
9	36848	33163	1,111118
10	27733	24960	1,111098
11	21399	19259	1,111117
L1 = 0,33 Lm L2 = 0,9 Lm			
Truss number	Tensile force without loss [N]	Tensile force with loss [N]	Ratio
2	58718	52847	1,111094
9	36848	33163	1,111118
10	27733	24960	1,111098
11	21399	19259	1,111117

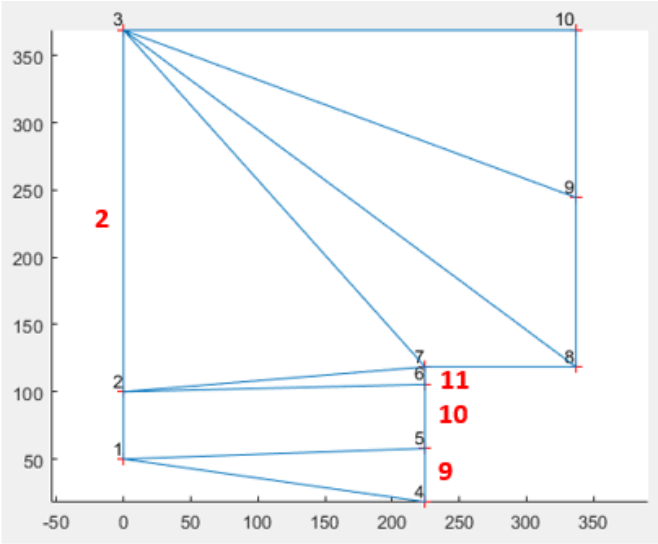

Figure 44 - Design of the R400L

6.3.3 Comparison between R400L and R400UL

When plotting Figure 38 and Figure 42 on the same graph, Figure 45 is obtained. As earlier mentioned, the relation between the percentage prestress loss and the corresponding fraction of the transmission length to obtain the same internal forces are the same for the R400L and R400UL. Because this relation is exactly the same it can be concluded that the upper reinforcement has no influence on these parameters. With these parameters is meant, by changing the lever arm the upper reinforcement has no influence on the internal forces of the strut-and-tie model. Nor will L2 influence these internal forces.

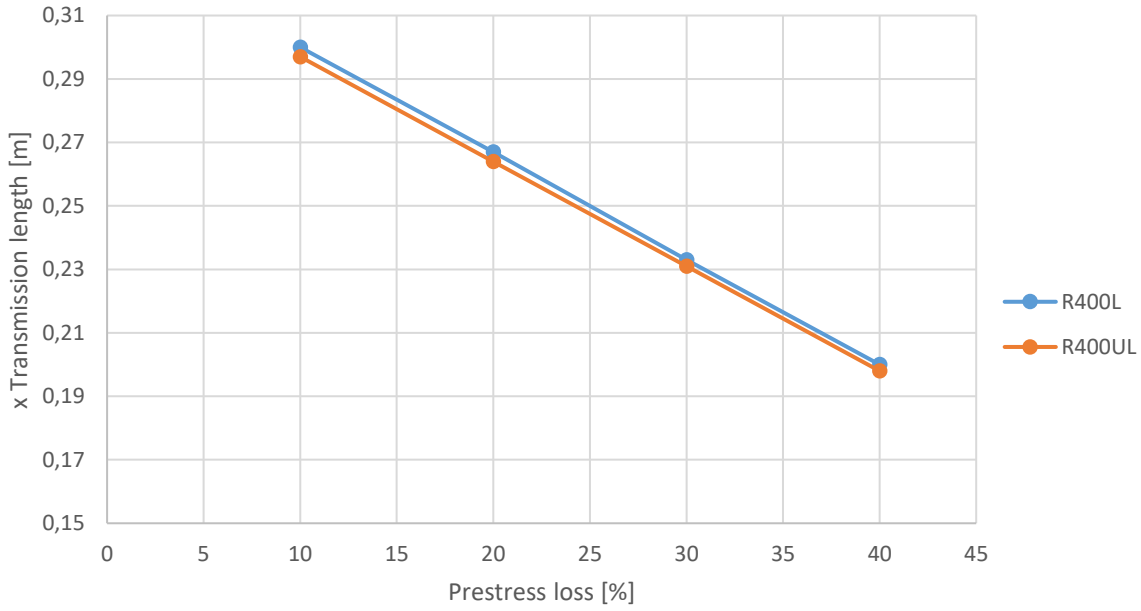

Figure 45 - The percentage prestress losses in function of the L1 lever arm (R400L & R400UL)

6.3.4 Comparison between R400UL and I700UL

When plotting Figure 38 and Figure 39 on the same graph, Figure 46 is obtained. This is once again the relation between the percentage prestress loss and the corresponding fraction of the transmission length to obtain the same internal forces. Also like in previous section, the relation between the R400UL and the I700UL are exactly the same. From Figure 46 it can be concluded that the geometry of the beam does not have an influence on these parameters. With these parameters is meant, by changing the lever arm, the upper reinforcement has no influence on the internal forces of the strut-and-tie model. This is because the properties of the geometry are already taken into account when generating the location of the nodes in the strut-and-tie model. Because the generating of these nodes will happen in the same manner for every beam, the geometry will have no influence on the relation displayed in Figure 46.

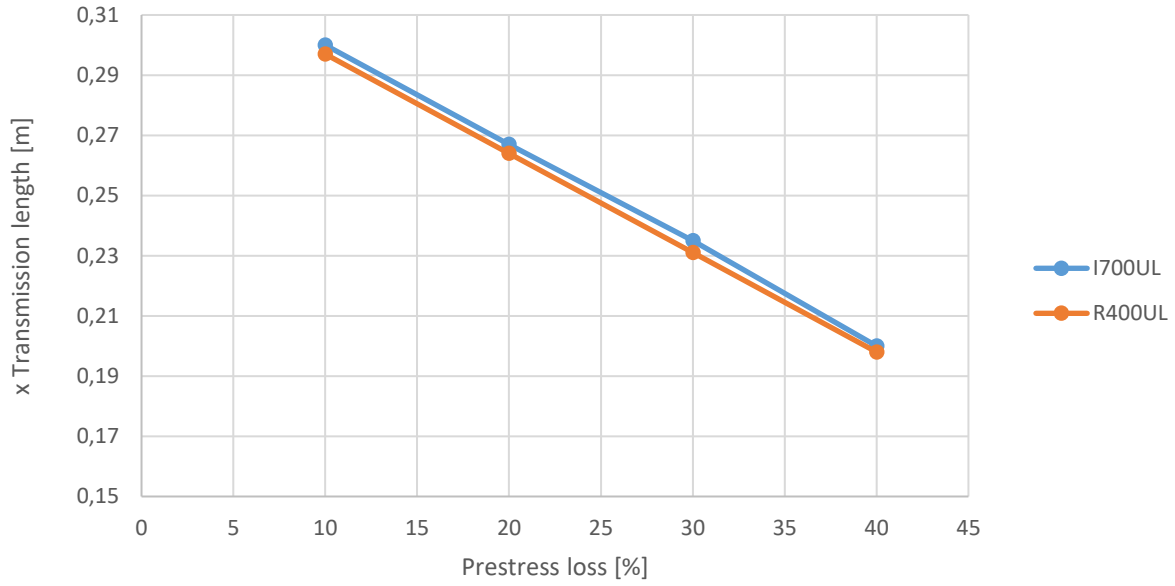

Figure 46 - The percentage prestress losses in function of the L1 lever arm (R400UL & I700UL)

6.3.5 Concluding remark

By comparing the R400L and the R400UL in section 6.3.3, it can be concluded that the upper reinforcement does not have an influence on the changing lever arm and as a result also no influence on the internal forces of the strut-and-tie model. When comparing the R400UL and the I700UL in section 6.3.4, it can be concluded that the geometry of the beam has no influence on the changing lever arm and as a result also no influence on the internal forces of the strut-and-tie model. It must be noticed that the geometry has no influence because the geometry has already been taken into account when the vertical location of the nodes are calculated. These calculations for the vertical location of the nodes will be conducted in the same way for every beam.

Knowing that the geometry of the beam and the upper tendons have no influence on the internal forces. And also knowing the relation between the prestress losses and the fraction of transmission length. This will make it possible to implement a safety factor for each different type of prestressed beam. In practice, this correlation can be used to design every type of beam by taking the necessary safety factors into account. This safety factor is then specifically optimised for that type of beam.

7 Optimisation of the strut-and-tie model

In this chapter an attempt is made to optimise the strut-and-tie model developed by R. Steensels [4]. In the first section the used beams to carry out this research are shown. The geometrical properties of the beams and the tendons are displayed. In section 7.2, a first attempt is made to optimise the strut-and-tie model by varying the lever arm of the model. The varying of this lever arm will result in different deformations, these deformations can be transformed into energy. When these different amounts of energy are compared, the most efficient model can be determined. In section 7.3, a second attempt is made to optimise the strut-and-tie model. The general geometry of the struts and ties are adapted to find a more efficient model. A first evaluation is made by looking to the deformation energy as used in section 7.2, a second evaluation is done by looking at the tensile forces of the ties.

7.1 Examined beams

In this paragraph the different beams that are used to carry out this research are shown. Some different I-girders have been used with different dimensions. Also two rectangular shaped beams are used in this research, one with upper and lower tendons and one with only lower tendons.

7.1.1 R400UL

Figure 47 shows the geometry of the R400UL element. This element has a width and height of 400mm. Eight prestressing strands are placed on the lower part, all with a diameter of 12,5mm and two prestressing strands are placed in the upper part of the beam with a diameter of 9,3mm. The concrete cover to the axis of the tendons is 50mm and the distance in between the tendon is also 50mm. If the spacing between the tendons is too small, a large prestress force could result in crushing of the concrete when the compressive strength of the concrete is exceeded. When the spacing between the tendons is too big, the pretensioning will be insufficient. This applies to all beams used in this research.

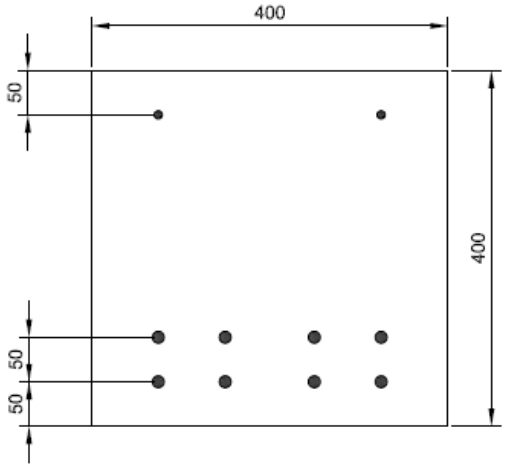

Figure 47 - Geometry of the R400 with upper and lower tendons [4, p. 107]

7.1.2 R400L

This beam has the same dimensions as the R400UL, only there are no upper tendons. These dimensions are again depicted on Figure 48. This element has a width and height of 400mm. Eight prestressing strands are placed on the lower part, all with a diameter of 12,5mm. The concrete cover to the axis of the tendons is 50mm and the distance in between the tendons is also 50mm.

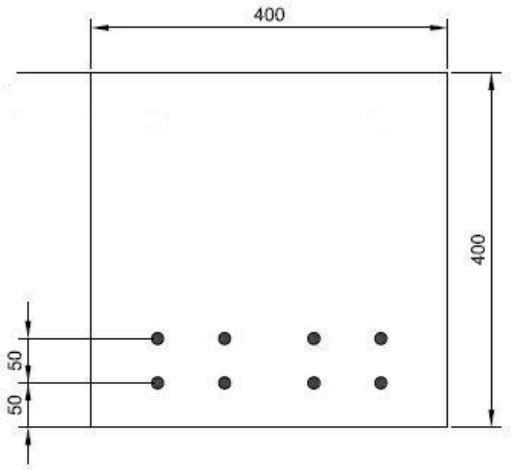

Figure 48 - Geometry of the R400 with lower tendons [4, p. 107]

7.1.3 IV1625

In Figure 49 the dimensions and the tendons of the IV1625 are depicted. This beam is IV-shaped with a width of 440mm and a total height of 978mm and has 24 prestressing strands with a diameter of 12,5mm. No upper tendons are used. IV-beams are beams that have a variable height and have a rectangular cross-section in the beginning in the anchorage zone. These beams are mainly used for roof structures.

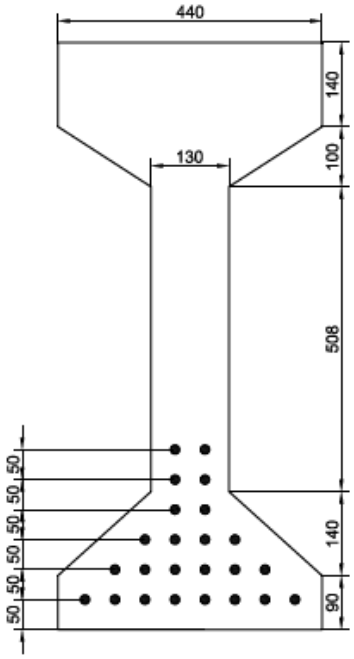

Figure 49 - Geometry of the IV1625 [4, p. 111]

7.1.4 I700

Figure 50 shows the dimensions of the I700 beam, the width is 290mm and has a total height of 700mm. All the prestressing strands have a diameter of 12,5mm, two strands are placed in the upper part of the beam and the other eight are placed on the bottom part of the beam. I-shaped beams are beams that have the same height and the same cross-section all over the length. These I-girders are mainly used for bridge applications.

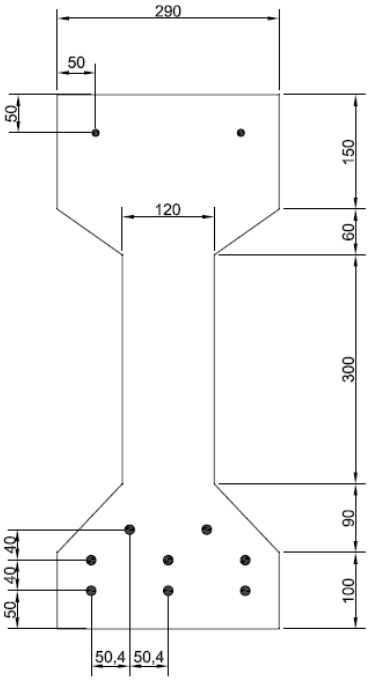

Figure 50 - Geometry of the I700 [4, p. 115]

7.2 Optimisation through the energy of the deformation of the trusses

In the next two paragraphs, two attempts are made to optimise the strut-and-tie model for the R400UL beam. The first attempt is made by using the same stiffness for each truss, trusses in tension and compression. Where trusses in tension are the reinforcement and trusses in compression the concrete. It is a simplified assumption that both the trusses in compression and tension have the same stiffness. In the second paragraph this stiffness for the trusses in tension is changed, another relation can be found and is explained in this second paragraph.

7.2.1 Same stiffness for each truss

The energy method will calculate the energy of the complete model. A natural state of the model can be assumed when the lowest energy is achieved. This low amount of energy will result in a more efficient distribution of the reinforcement. The energy of the complete model is calculated by determining the elongation of each truss element and multiplying it by the acting force in these trusses. Summing up all small parts of energy for each truss will give a total amount of energy. This total amount of energy can be used to describe the model in terms of optimal use of the materials.

To determine the energy in each truss in practice the following steps are made. The initial coordinates of each truss element is determined, when both coordinates are known, the length of the initial truss can be calculated:

$$initialLength = \sqrt{(x_1 - x_2)^2} + \sqrt{(y_1 - y_2)^2} \tag{7.1}$$

Equation 7.1 is also used to determine the length after the deformation of the truss, this parameter is named newLength. The elongation can be calculated as displayed in equation 7.2.

$$\varepsilon = \frac{(newLength - initialLength)}{initalLength} \tag{7.2}$$

The forces in each truss element can be calculated by using a numerical model, multiplying these forces by the elongation obtained in equation 7.2 the energy W can be calculated:

$$W = \varepsilon \,.\, F \tag{7.3}$$

When all the trusses' energy are calculated and summed up, a different amount of total energy is obtained when varying the transmission length. As expected an asymptote is obtained and is depicted in Figure 51. Figure 51 shows the relation between the energy of the model and the fraction of the transmission length. Lm, also known as the transmission length which is the distance needed in the beam to reach a linear distribution of stresses. When this parameter reaches a value of one times Lm, the asymptote will be smoothed out because from here on the Bernoulli area is reached. The beam can now again be calculated by using simple beam theory.

These results cannot be used to determine the optimal transmission length because it can be concluded that the lowest energy is achieved at an infinite transmission length which is not possible. This is due to the stiffness which is the same for the concrete and the reinforcement. When cracking occurs, a reduction of the stiffness should be taken into account. But it is very difficult to predict where cracking will occur and what the stiffness will be after cracking.

When looking at Figure 51 one data point jumps out of the curve. Here a transmission length of 0,55 times the transmission length is reached. The energy that corresponds to this fraction of 0,55 times the transmission length is a lot lower than the rest of the asymptote. Seeing this value might tell that this leads to the most efficient transmission length to design the anchorage zone. Unfortunately this is just a discrepancy in the software and is not an optimal point where the lowest energy is obtained.

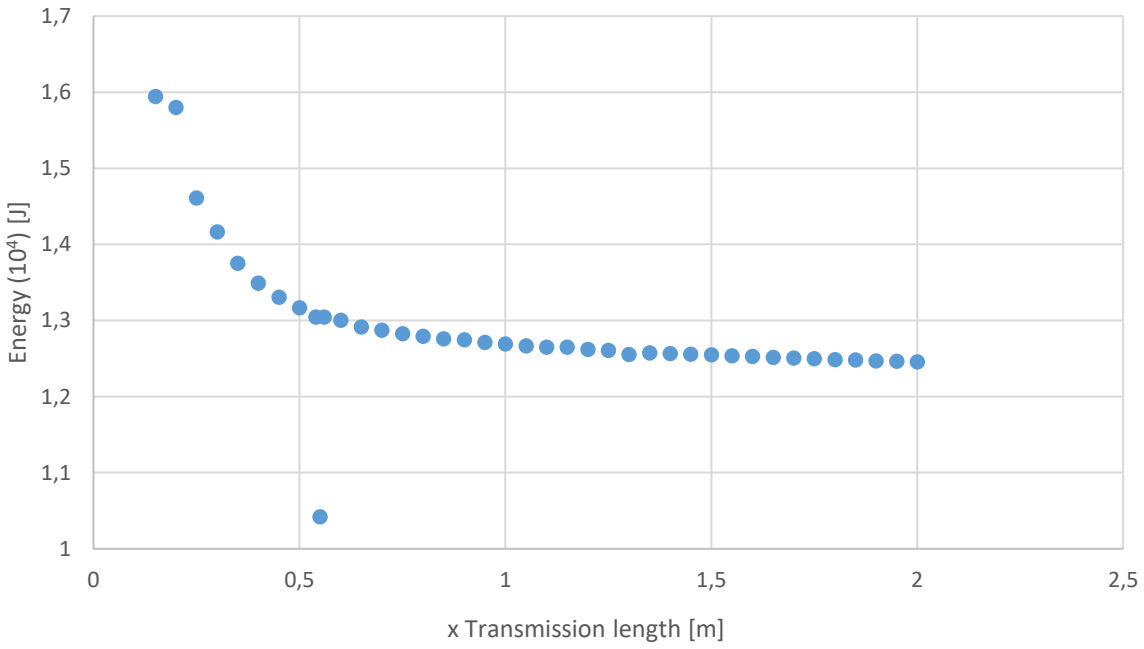

Figure 51 - Energy of the strut-and-tie model in function of the transmission length with the same stiffness

7.2.2 A different stiffness for trusses in tension

In section 7.2.1 the optimisation did not succeed. This might have been because the stiffness for the concrete and reinforcement were the same. Also when cracking occurs, a reduction of stiffness should be taken into account. A next attempt is to change the stiffness in the trusses that are in tension, the ties. It is likely that cracking will occur at almost the same location of the ties. It is difficult to determine the exact stiffness of the truss in each different element and is not apprehended in this research. A stiffness of 100 times smaller in the ties than the original stiffness is tested to see if an optimal point can be found. The results are displayed on Figure 52. Figure 52 shows the relation between the fraction of the transmission length with the corresponding amount of energy of the model.

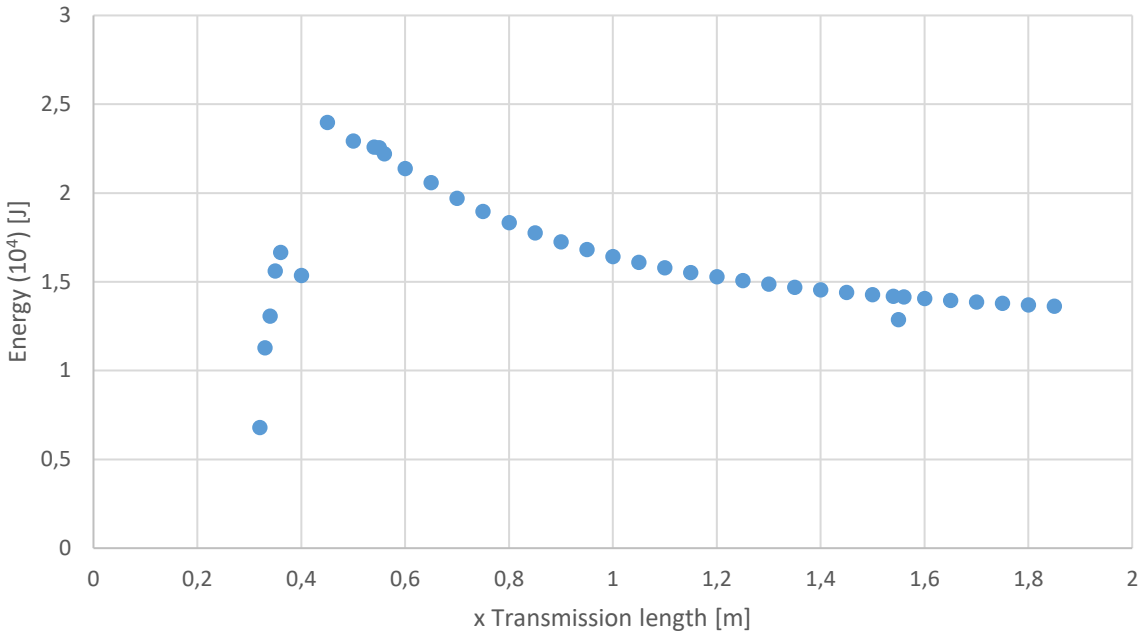

Figure 52 - Energy of the strut-and-tie model in function of the transmission length with varying stiffness

As can be seen on Figure 52 the lowest energy is obtained with a fraction of 0,32 times the transmission length. A small drop back can be found at a fraction of 0,4 times the transmission length. When smaller fractions than 0,32 times the transmission length are tested the energy will become negative. This negative energy is not a logical result of a lower transmission length and is left out of the graph. Again, when the full transmission length is reached, the graph is smoothed out.

7.2.3 Concluding remark

The obtained value of L1 = 0,32Lm approximates the value of L1 = 0,33Lm used in the doctorate's thesis of R. Steensels and was already almost an optimal use of the leverage arm [4]. A further optimisation through this method is probably not possible. Maybe by better modelling the stiffness of the trusses by predicting the cracking patterns may result in a more exact solution for this leverage arm.

7.3 Strut-and-tie model designed by A. Schraeyen and L. Vanbuel

In this section another attempt is made to optimise the strut-and-tie model of the IV1625. The overall geometry is adapted to achieve this objective. Eight different proposals are examined and are shown in Appendix A. In section 7.3.1 the first attempt is made to optimise the model by comparing the energy of all the different proposals. In section 7.3.2 a new plan of approach is used. The total amount of the tensile forces of each proposal is compared.

7.3.1 Geometric optimisation through the deformation energy

A first guide value to optimise the strut-and-tie model designed by R. Steensels [4] was to look at the total energy of the model. By adding an extra truss depicted on Figure 53, from node 18 to 23, a more efficient model is achieved in terms of energy. The total amount of energy of this system is 441 Joule. While the energy of the model used in the research of R. Steensels amounts 14,98kJ. But when looking at the internal forces of the ties, no differences are observed. This means that the total vertical reinforcement will remain the same. The reason why the energy of proposal 1 might be lower is that a more stiff design is created. As a result, the deformations will be smaller and this will result in a lower energy because energy is the multiplication of the forces and the deformations. Like mentioned before, the forces remained the same so only the deformations could have changed. When comparing Figure 54 and Figure 55 it can be confirmed that the deformations of proposal 1 are smaller. To still find a more efficient model a new approach is needed. In the next section the total amount of tensile forces between different proposals will be compared.

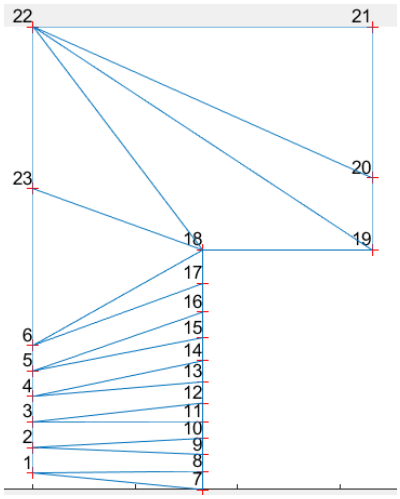

Figure 53 - Strut-and-tie model proposal 1

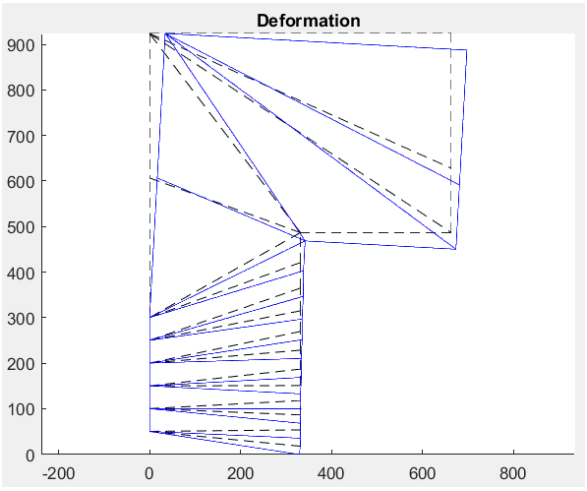

Figure 54 - Deformation proposal 1

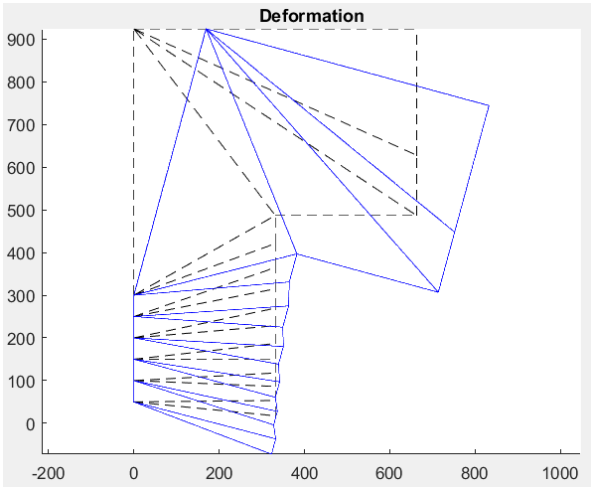

Figure 55 - Deformation of R. Steensels' model

7.3.2 Geometric optimisation by comparing the sum of tensile forces

Because the previous method was no success to a more efficient model, a different approach is used. First, all the proposals were executed and the total amount of tensile forces for each proposal were summed up. The one with the lowest amount of tensile forces is further examined. When looking at

Table 5 the results for the different proposals can be found. Number 9 is the total tensile force of the model of R. Steensels which is used as reference (Ref) [4]. Proposal 7 has a total tensile force of 596,47kN, R. Steensels' model is only having a slight lower total tensile force of 512,36kN. This proposal, number 7, is further examined.

Table 5 – Tensile forces for each proposal

Proposal	Tensile force [kN]
1	927,06
2	1344,20
3	659,86
4	1823,60
5	620,28
6	1290,50
7	596,47
8	2659,50
Ref	512,36

The design of proposal number 7 is depicted on Figure 56 on which the truss numbers are displayed in red. Now the different ties can be compared, the ties are subdivided in spalling- and bursting ties. Table 6 displays the diagonal oriented, spalling and bursting ties with the corresponding truss number and tensile force to that specific truss for proposal 7. Table 7 displays the same as Table 6 except these are the values in accordance with R. Steensels' model [4]. The design of this model is shown in Figure 57.

Table 6 – Tensile forces proposal 7

Proposal 7		
	Truss number	Tensile force [kN]
Spalling	16	50,40
Diagonal	31	76,76
Bursting	19	71,38
	26	268,13

Table 7 – Tensile forces model R. Steensels

R. Steensels' model (Ref)		
	Truss number	Tensile force [kN]
Spalling	16	107,67
	13	48,01
	10	13,13
Diagonal	32	97,79
Bursting	20	25,35
	19	22,74
	21	30,86
	26	20,33
	22	20,13
	27	5,69
	23	0,13

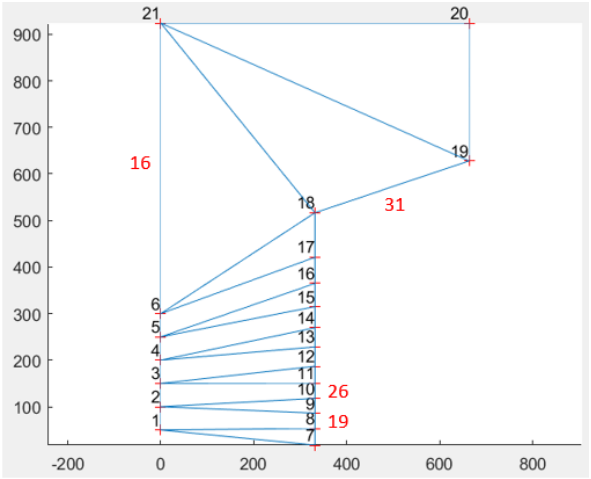

Figure 56 - Strut-and-tie model proposal 7

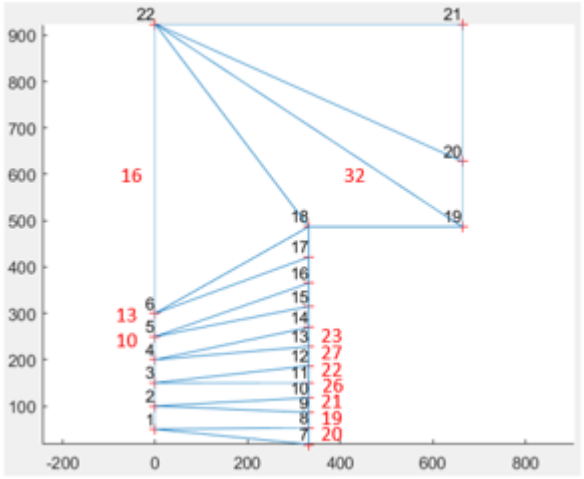

Figure 57 - Strut-and-tie model R. Steensels

When summing up the spalling forces for Table 6 and Table 7, a total amount of spalling force of respectively 50,40kN and 168,81kN is obtained. As can be seen, the total amount of spalling force for proposal 7 is a lot smaller. But when comparing the bursting force of the two models, a bursting force of 339,51kN and 125,23kN for respectively proposal 7 and R. Steensels' model is obtained. Concluding, the spalling forces for proposal 7 are smaller but the bursting forces are much higher.

7.3.3 Reinforcement design based on STM

After determining the tensile forces in the vertical direction, the reinforcement can be calculated according to the formula $A = \frac{F}{f_y}$. The safety factors must be taken into account as specified in section 6.1. Vertical reinforcement must be placed to interact the tensile stresses named busting and spalling which are shown in Figure 58. Spalling occurs at the end face of the beam and bursting occurs at the lower part of the beam at a specified distance from the end of the beam. An example of the vertical reinforcement is shown in Figure 59. Only half the reinforcement is depicted in the figure below due to symmetry.

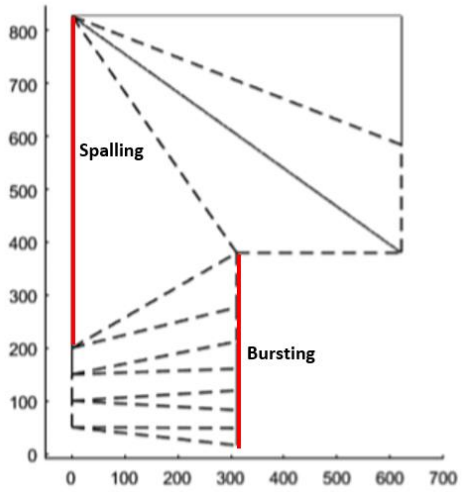

Figure 58 - Bursting and spalling

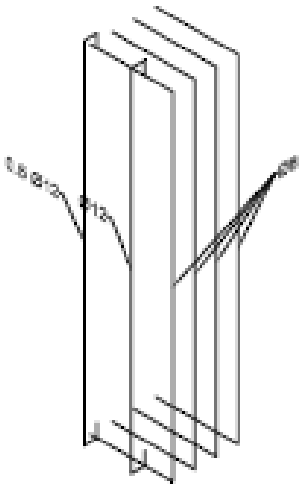

Figure 59 - Example placing reinforcement IV1625 [4, p. 112]

8 Conclusion

Because prestressed concrete is becoming more common in construction works, it is necessary to have a better knowledge of the different cracks occurring due to the prestressing. To better understand these cracking patterns a numerical model of the beam is developed and afterwards a strut-and-tie model is designed based on this numerical model.

The first goal of this master's thesis is to find a correlation to obtain the same reinforcement as before the prestress loss is applied by analysing the strut-and-tie model. This correlation will make it possible to serve as an initial safety factor. Because this initial safety factor will probably not suffice, another safety factor will be defined to apply to the prestress force. The final goal of this research is to optimise the strut-and-tie model provided by R. Steensels [4]. Two methods are used to optimise this strut-and-tie model. A first approach is by calculating the deformation of the struts and ties and multiplying it by the force in each strut and tie. This translates into the energy dissipated in this model. The lowest amount of energy would result in the most efficient strut-and-tie model. A second approach consists of redesigning the strut-and-tie model provided by R. Steensels. This is done by relocating and adding several struts and ties.

First, a correlation between the percentage prestress loss and the necessary reduction of the transmission length or the lever arm is found to maintain the same reinforcement. This relation is as follows and is only valid for the strut-and-tie model used in this research:

$$Fraction\ transmission\ length = -0{,}0033 * (Percentage\ prestress\ loss) + 0{,}3335$$

Because the geometry is already taken into account when calculating the position of the nodes in the strut and tie model, the outcome of this correlation will be the same for every beam geometry used. When comparing beams with upper and lower reinforcement with beams with only lower reinforcement, also the same correlation can be found. In practice, this equation can be used to adapt the lever arm depending on the percentage prestress loss to maintain the same amount of reinforcement. This will serve as a safety factor for the prestress losses only due to the immediate effects.

Second, in chapter 0, all the different prestress losses are explained. Only the immediate losses are worth taking into account because the effects of prestressing will act immediately after cutting the tendons. These immediate losses can be subdivided in the elastic shortening of the concrete, friction between the tendons and the concrete and the anchorage slip. N. Raju [24] mentions that a 25% loss will occur in pretensioning a beam. While Eurocode 0 [22] mentions that a safety factor of 1,3 should be used when the prestressing is unfavourable, which is highly recommended in this research.

Next, an attempt is made to optimise the strut-and-tie model provided by R. Steensels by changing the lever arm. A first approach was to optimise the STM by calculating the deformation energy of the model and keeping the same stiffness for the struts and ties. This resulted in a minimal energy at an infinite length of the lever arm which is not realistic. Thereafter, the stiffness for the ties are adapted because after cracking of the concrete a lower stiffness is obtained. An optimal lever arm has been found at 0,32 times the transmission length. R. Steensels used a lever arm of 0,33 times the transmission length which approximates the value of 0,32. No real optimisation could be implemented.

Finally, a different angle is used to optimise the strut-and-tie model. The complete geometry of the model is adapted by relocating and adding struts and ties. Eight proposals were conducted in this research and compared with R. Steensels' model. All different proposals resulted in a higher total tensile force. Only one proposal almost equalled the proposal of R. Steensels, this model is further examined but a fully optimised model is not found.

Future perspectives

In order to make the model practically usable, some adjustments have to be made. It has to be validated that the model provided by R. Steensels [4] is the same for every type of beam. Next, this model can be programmed and a user-friendly interface can be used where the geometry, the prestress force, type of concrete, etc. is inserted. It would also be possible to write a guideline to design the end-zone reinforcement of these beams but a fully automated software will be much more convenient. The correlation for the usage of safety factors determined in this thesis could also be implemented. Up to now, the model only calculates the internal forces in the struts and ties. The forces in the ties can be converted into reinforcing areas. When the reinforcing area is calculated, the placement of the reinforcement should also be determined and displayed. The vertical reinforcement calculated in this research, to prevent bursting and spalling cracks, will also act as shear reinforcement. It would also be an opportunity to calculate the supplementary shear reinforcement to prevent shear failure. This will make it possible to make one drawing with all the necessary reinforcement displayed. The drawing could easily be printed out and used to be manufactured in the construction hall.

A further optimisation is still necessary, the model of R. Steensels is already a very optimal design. When further optimising the model, a lower amount of reinforcement on a more efficient placement could be determined. This will make it advantageous for manufacturers to invest in the software to design this end-zone reinforcement. Another approach will have to be used, than used in this research. A possibility to reach a more optimal design is to implement more realistic stiffnesses in the model when validating the deformation energy.

A last step in the process is to test several beams by using the most efficient model. The crack patterns and also the transfer of the prestressing force should be analysed. When everything is validated, a software program could be written like explained previously. This software program will make it possible to optimise all the vertical reinforcement to prevent spalling and bursting cracks in a very efficient way. When a sufficient reduction of the end-zone reinforcement is achieved which is feasible and trustworthy, the manufacturers will very likely start using this method for designing the end-zone reinforcement of these girders.

Bibliography

[1] “Details research group Construction engineering (CERG),” UHasselt, 2018. [Online]. Available: https://www.uhasselt.be/UH/Research-groups/Details-research-group.html?oid=1875. [Accessed 11 May 2018].

[2] “Elements for structural works and bridges,” Ergon, 2018. [Online]. Available: https://www.ergon.be/en/products/elements-for-structural-works-and-bridges/. [Accessed 11 May 2018].

[3] “Prefab Beton Voordelen,” FEBE, 2018. [Online]. [Accessed 12 May 2018].

[4] R. Steensels, “Efficient End-Zone detailling of Pre-Tensioned Concrete Elements,” Diepenbeek, Belgium, 2018.

[5] CEB-FIP, “Model Code2010 Volume 2,” International Federation for Structural Concrete (fib), Case Postale 88, CH-1015 Lausanne, Switzerland, April 2010.

[6] E. D. Crispino, “Anchorage zone design for pretensioned precast bulb-T bridge girders in Virginia,” VTRC, Virginia, June 2009.

[7] Caltrans, “Precast pretensioned concrete girders,” February 2015. [Online]. Available: http://www.dot.ca.gov/des/techpubs/manuals/bridge-design-practice/page/bdp-8.pdf.

[8] M. F. Sulaiman, “A review on Bond and Anchorage of COnfined High-strength Concrete,” Elsevier, Department of structure and materials, Faculty of Civil Engineering, Universiti Teknologi, Malaysia, 2017.

[9] C. Williams, “Strut- and-Tie model Design Examples for Bridges: Final Report,” The University of Texas at Austin, 1616 Guadalupe, Suite 4.202, Austin, TX 78701, 2011.

[10] A. Shah, “Analysis and Design of Disturbed Regions in Concrete Structures,” Elsevier, Hazara University Mansehra Pakistan, 2011.

[11] “mpa The Concrete Centre,” [Online]. Available: http://www.concretecentre.com/Concrete-Design/Design-Codes/Eurocode-2/Stut-and-Tie.aspx. [Accessed 29 9 2017].

[12] Eurocode, Eurocode 2: Ontwerp en berekening van betonconstructies -Deel 1-1: Algemene regels en regels voor gebouwen (+AC:2010), Birminghamstraat 131, 1070 Brussel, 2010.

[13] AASHTO, “Standard Specifications for Highway Bridges,” Wahington, D.C., 2002.

[14] D. Whelan, “In-Class Demonstration: Saint-Venant's Principle and Stress Concentrations,” 2010.

[15] Mattock, “Control of horizontal cracking in the ends of pretensioned prestressed concrete girders,” 1962.

[16] P. Gergely, “Design of anchorage-zone reinforcement in prestressed concrete beams,” PCI Journal, 1967.

[17] C. Y. Tuan, “End zone reinforcement for pretensioned concrete girders,” University of Nebraska, Omaha, 2004.

[18] D. Mitchell, “Influence of high strength concrete of transfer and development length of pretensioning strand,” PCI Journal 38, 1993.

[19] B. H. Oh, “Theoretical analysis of transfer lengths in pretensioned prestressed concrete members,” Journal of Engineering Mechanics 132, 2006.

[20] M. R. O'Callaghan, “Tensile stresses in the end regions of pretensioned I-beams at release,” University of Texas, Texas, 2007.

[21] Eurocode, Eurocode 1: Belastingen op constructies, Birminghamstraat 131, 1070 Brussel: Bureau voor Normalisatie, 2015.

[22] Eurocode, “Eurocode 0: Grondslag voor het constructief ontwerp,” NBN, Birminghamstraat 131 1070 Brussel, 2013.

[23] D. Menon, “Prestressed concrete structures,” Indian Institute of Technology Madras.

[24] N. K. Raju, “Prestressed concrete,” Tata McGraw-Hill Pub.Co., New Delhi, 2007.

[25] CEB-FIP, “Model Code 1990,” Thomas Telford, Case Postale 88, CH1015 Lausanne, Switzerland, 1993.

[26] S. Nipun, “What is oligopoly?,” Economics discussion, [Online]. Available: http://www.economicsdiscussion.net/oligopoly/what-is-oligopoly-markets-economics/25723. [Accessed 23 May 2018].

Appendix

Appendix A: Different proposals

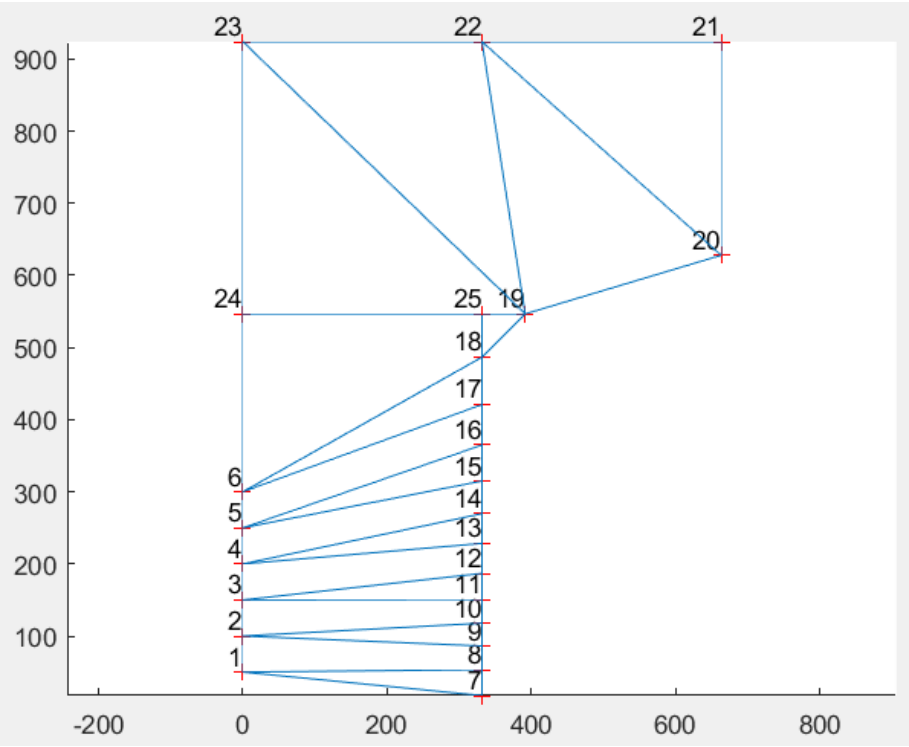

Figure 60 - Proposal 1

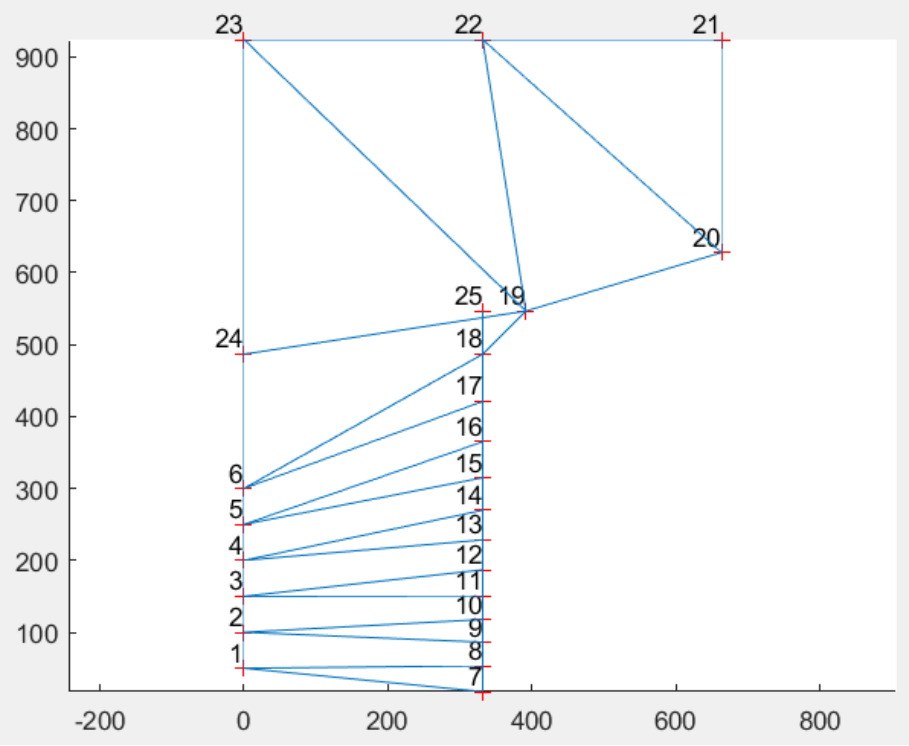

Figure 61 - Proposal 2

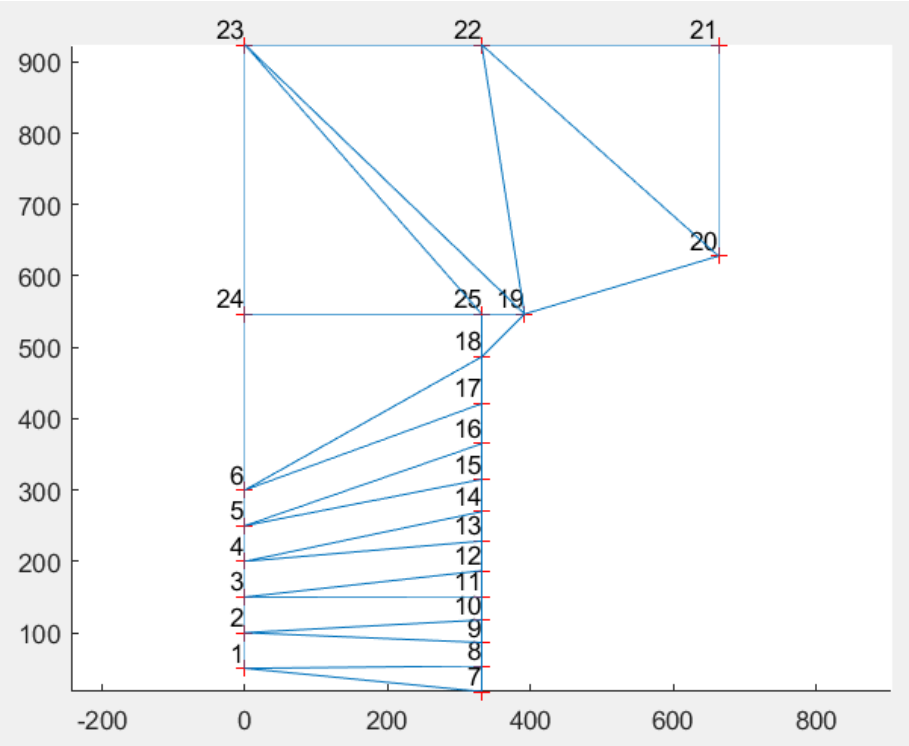

Figure 62 - Proposal 3

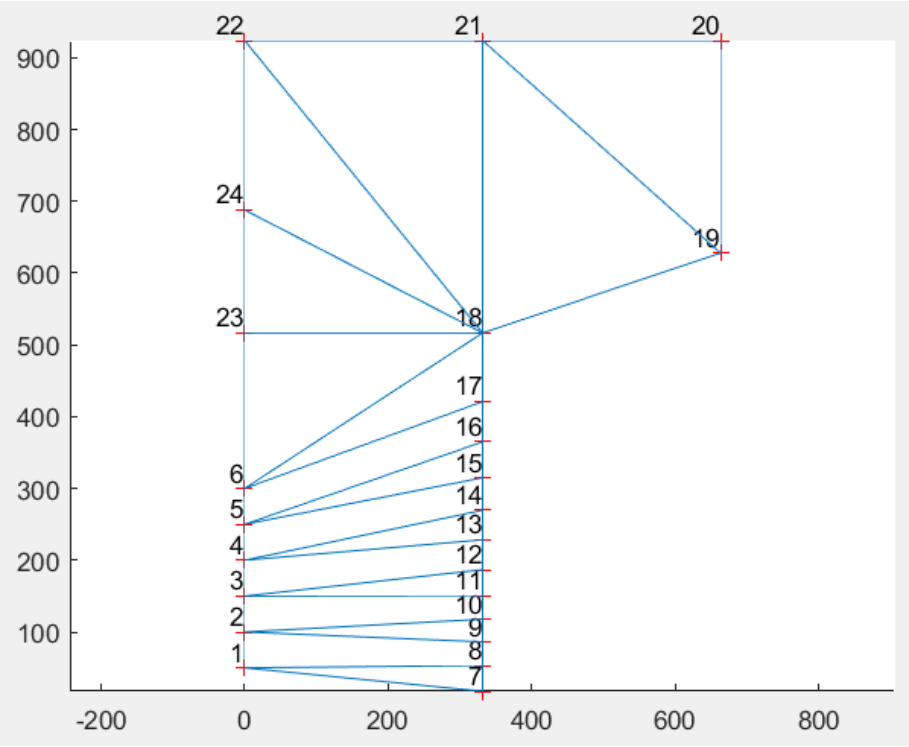

Figure 63 - Proposal 4

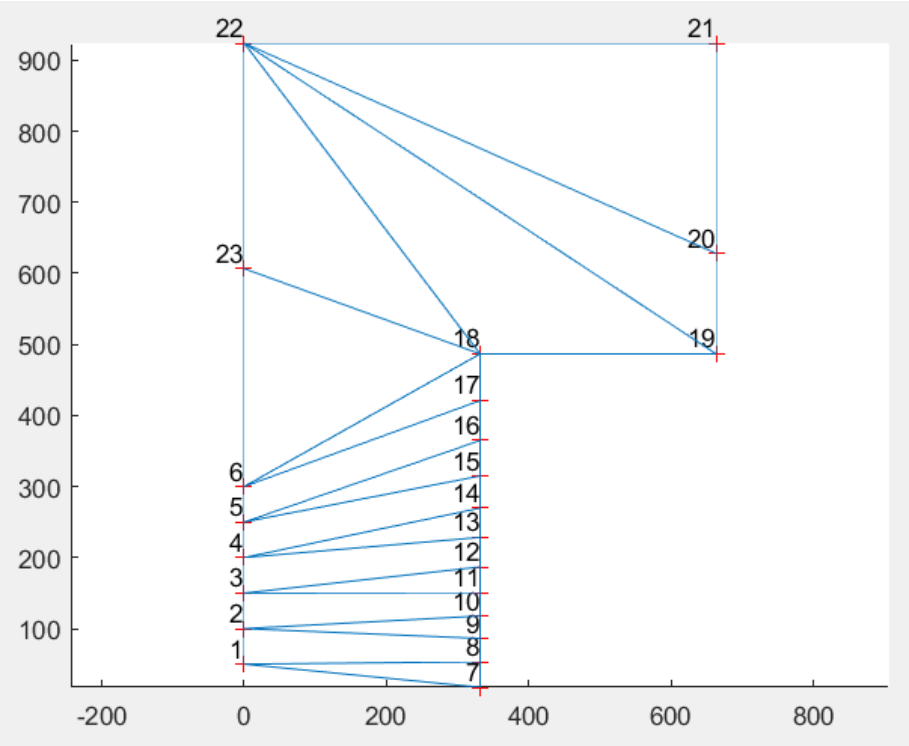

Figure 64 - Proposal 5

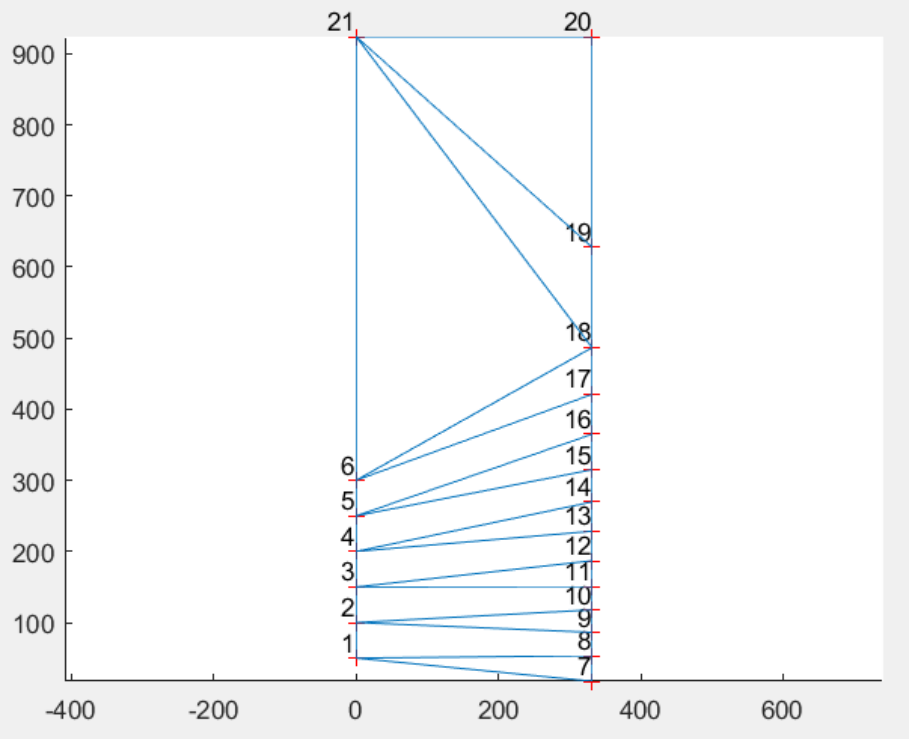

Figure 65 - Proposal 6

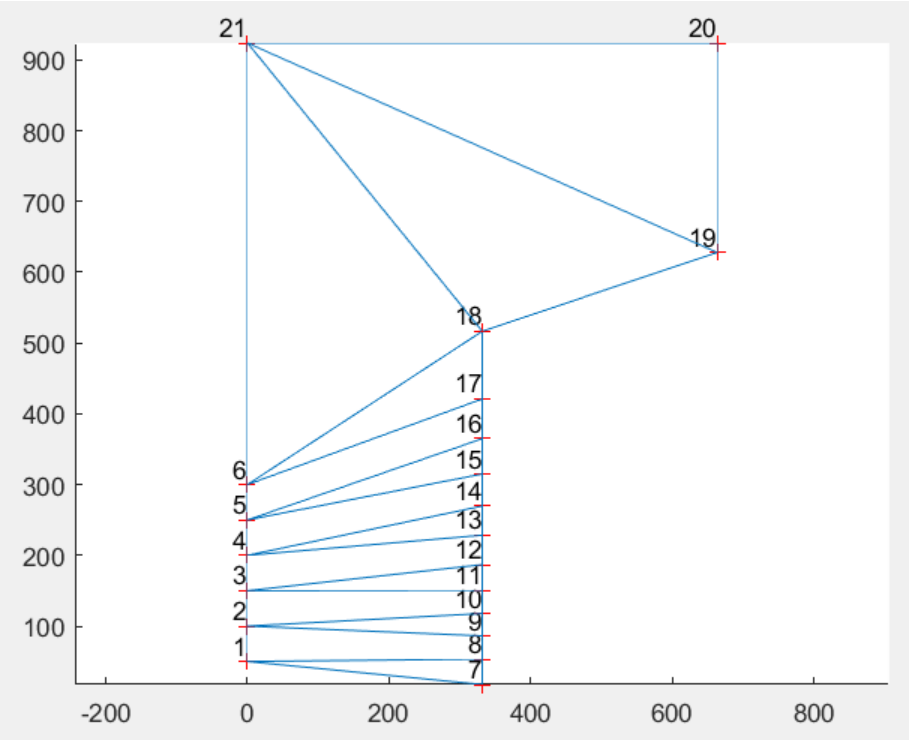

Figure 66 - Proposal 7

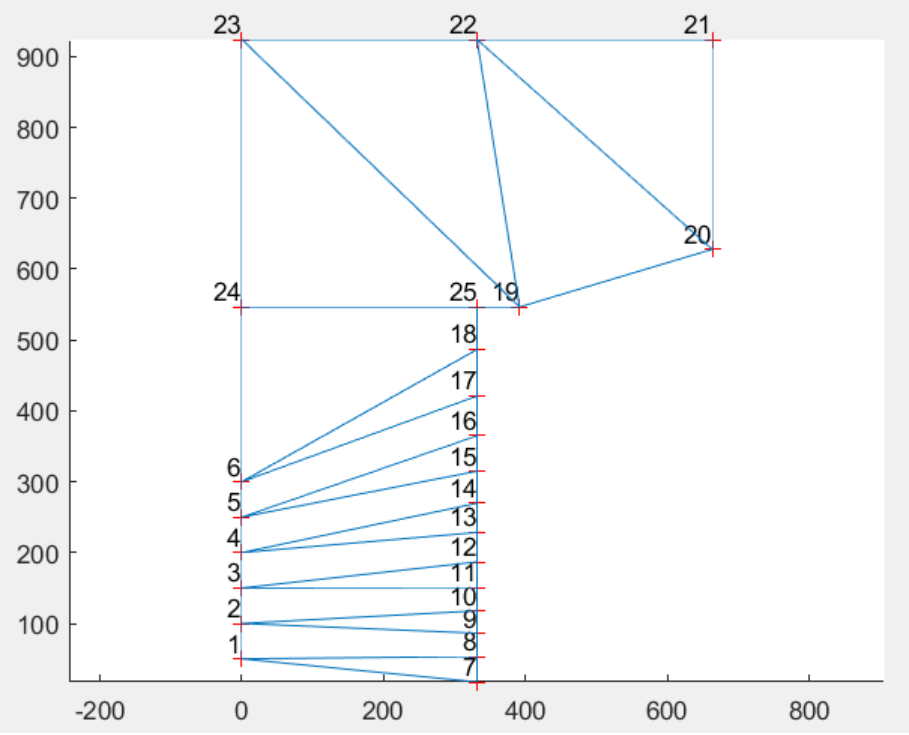

Figure 67 - Proposal 8

Auteursrechtelijke overeenkomst

Ik/wij verlenen het wereldwijde auteursrecht voor de ingediende eindverhandeling:
Modelling of the anchorage zone of prestressed concrete elements

Richting: **master in de industriële wetenschappen: bouwkunde**
Jaar: **2018**

in alle mogelijke mediaformaten, - bestaande en in de toekomst te ontwikkelen - , aan de Universiteit Hasselt.

Niet tegenstaand deze toekenning van het auteursrecht aan de Universiteit Hasselt behoud ik als auteur het recht om de eindverhandeling, - in zijn geheel of gedeeltelijk -, vrij te reproduceren, (her)publiceren of distribueren zonder de toelating te moeten verkrijgen van de Universiteit Hasselt.

Ik bevestig dat de eindverhandeling mijn origineel werk is, en dat ik het recht heb om de rechten te verlenen die in deze overeenkomst worden beschreven. Ik verklaar tevens dat de eindverhandeling, naar mijn weten, het auteursrecht van anderen niet overtreedt.

Ik verklaar tevens dat ik voor het materiaal in de eindverhandeling dat beschermd wordt door het auteursrecht, de nodige toelatingen heb verkregen zodat ik deze ook aan de Universiteit Hasselt kan overdragen en dat dit duidelijk in de tekst en inhoud van de eindverhandeling werd genotificeerd.

Universiteit Hasselt zal mij als auteur(s) van de eindverhandeling identificeren en zal geen wijzigingen aanbrengen aan de eindverhandeling, uitgezonderd deze toegelaten door deze overeenkomst.

Voor akkoord,

Schraeyen, Alexander **Vanbuel, Lennert**

Datum: **3/06/2018**